Microphysics of Clouds with the Relaxed Arakawa–Schubert Scheme (McRAS). Part I: Design and Evaluation with GATE Phase III Data

Y. C. SUD AND G. K. WALKER*

Climate and Radiation Branch, Laboratory for Atmospheres, NASA/Goddard Space Flight Center, Greenbelt, Maryland

(Manuscript received 9 June 1997, in final form 3 November 1998)

ABSTRACT

A prognostic cloud scheme named McRAS (Microphysics of Clouds with Relaxed Arakawa–Schubert Scheme) has been designed and developed with the aim of improving moist processes, microphysics of clouds, and cloud–radiation interactions in GCMs. McRAS distinguishes three types of clouds: convective, stratiform, and boundary layer. The convective clouds transform and merge into stratiform clouds on an hourly timescale, while the boundary layer clouds merge into the stratiform clouds instantly. The cloud condensate converts into precipitation following the autoconversion equations of Sundqvist that contain a parametric adaptation for the Bergeron–Findeisen process of ice crystal growth and collection of cloud condensate by precipitation. All clouds convect, advect, as well as diffuse both horizontally and vertically with a fully interactive cloud microphysics throughout the life cycle of the cloud, while the optical properties of clouds are derived from the statistical distribution of hydrometeors and idealized cloud geometry.

An evaluation of McRAS in a single-column model (SCM) with the Global Atmospheric Research Program Atlantic Tropical Experiment (GATE) Phase III data has shown that, together with the rest of the model physics, McRAS can simulate the observed temperature, humidity, and precipitation without discernible systematic errors. The time history and time mean in-cloud water and ice distribution, fractional cloudiness, cloud optical thickness, origin of precipitation in the convective anvils and towers, and the convective updraft and downdraft velocities and mass fluxes all simulate a realistic behavior. Some of these diagnostics are not verifiable with data on hand. These SCM sensitivity tests show that (i) without clouds the simulated GATE-SCM atmosphere is cooler than observed; (ii) the model's convective scheme, RAS, is an important subparameterization of McRAS; and (iii) advection of cloud water substance is helpful in simulating better cloud distribution and cloud–radiation interaction. An evaluation of the performance of McRAS in the Goddard Earth Observing System II GCM is given in a companion paper (Part II).

1. Introduction

It has been variously emphasized that an accurate representation of clouds is vital for simulating realistic prognostic cloud-radiative forcing in a general circulation model (GCM). However, because cloud production and dissipation processes are very sensitive to the vertical structure of temperature and humidity, the requirement places an enormous demand on the accuracy of almost all the physical parameterizations that affect the atmosphere. To circumvent this problem, particularly in the early stages of climate model development, clouds and their optical properties were climatologically prescribed (e.g., Washington and Kasahara 1970; Manabe and Holloway 1971) or inferred in highly idealized ways, for example, the entire grid cell was assumed to be cloudy (clear) if precipitation was (was not) occurring, as in Arakawa (1972). As the performance of moist processes in GCMs improved, more detailed physics was invoked into the cloud models. A chronological review and a comprehensive discussion of different cloud schemes can be found in Fowler et al. (1996).

Sundqvist (1978) devised a parameterization for fractional cloudiness of nonconvective clouds with in-cloud condensation and evaporation; it was the first attempt to transform cloud water into precipitation microphysically. With suitable approximations of cloudy and cloud-free conditions, Sundqvist (1988) was able to emulate fractional clouds in a large-scale environment with an average relative humidity of less than 100%, a frequent occurrence on a typical GCM grid scale. These concepts were utilized by LeTreut and Li (1988) and Sundqvist et al. (1989), who were among the pioneers to include a prognostic cloud water scheme into their GCMs. Randall (1989) provided an exhaustive discus-

* Current affiliation: General Sciences Corporation, Laurel, Maryland.

Corresponding author address: Dr. Yogesh C. Sud, Climate and Radiation Branch, Laboratory for Atmospheres, NASA/Goddard Space Flight Center, Greenbelt, MD 20771.
E-mail: sud@climate.gsfc.nasa.gov

sion of the issues that need to be addressed for improving the cloud parameterization and cloud–radiation interaction in GCMs. Fowler et al. (1996) gave a comparative review of the key features of three classes of cloud schemes while Del Genio et al. (1996) critically discussed the cloud-radiative issues of a hierarchy of cloud schemes that have been adopted by various well-known modeling groups. Subsequently, a few more prognostic cloud water schemes have appeared due to Zhao and Carr (1997), Cheng and Arakawa (1997), and Rasch and Kristjánsson (1998). Despite substantial progress in cloud parameterization, there remain several unresolved issues that require future research and development. This is evident in the comparison of simulated clouds versus observed (e.g., Fowler and Randall 1996a,b; Del Genio et al. 1996). Xu and Randall (1996) contend that cloud problems emanate from lack of resolution, inadequate representation of subgrid-scale effects, and the inability of cloud parameterizations to redistribute momentum, heat, and moisture properly. Consequently, we have paid special attention to representation of physical details of the subgrid-scale cloud structures and have designed algorithms to represent some of them more realistically than currently.

Cloud processes have four major components: (i) in-cloud condensation and evaporation; (ii) autoconversion, growth of ice-crystals by Bergeron–Findeisen process (Bergeron 1935), and condensate collection by falling hydrometors; (iii) phase change of precipitation during fall including its evaporation or sublimation with its plausible consequences, that is, precipitation-induced downdrafts; and (iv) cloud-radiative forcing based on the optical properties of cloud extent and cloud water/ice content. In Part I, we discuss the synthesis of the moist processes containing the Relaxed Arakawa–Schubert cumulus Scheme (RAS; Moorthi and Suarez 1992) with two new parameterizations—one for stratiform and one for boundary layer condensation into a new cloud microphysics complex named the Microphysics of clouds with Relaxed Arakawa–Schubert Scheme (McRAS). McRAS was evaluated with Global Atmospheric Research Program Atlantic Tropical Experiment GATE Phase III (hereafter GATE) data in a single-column model (SCM).

Most of the earlier prognostic cloud schemes ignored the cloud microphysical processes in convective towers and anvils and the associated cloud-radiation effects. In McRAS we carry cloud microphysics into convective towers as well. Our treatment of stratiform condensation heating implicitly conveys to the entire grid cell, which occurs in nature on subgrid scales via cloud ascent and environment subsidence. The primary goal of our work is to construct a parametric design that works without discernible systematic biases in the seasonal mean and the annual cycle of cloudiness, cloud-radiative forcing, precipitation, and atmospheric water vapor fields. We contend that if the above goals are achieved, the scheme is likely to perform satisfactorily in climate simulation studies. This contention is based on general understanding of the performance of GCMs. For example, Gadgil and Sajani (1997) noted that the Atmospheric Model Intercomparison Project models that simulated a better mean climate and seasonal movement of the ITCZ also did well in simulating the interannual variability of monsoons. The rest of the paper is organized as follows. Section 2 shows the design features of McRAS. Section 3 describes the evaluation procedure in an column model (SCM). Section 4 shows results of SCM evaluation and four sensitivity studies to assess the importance of convection and cloud-radiative forcing, and section 5 concludes with a summary of the results. McRAS was subsequently implemented and evaluated in the 4° latitude $\times$ 5° longitude $\times$ 20 sigma layer version of the Goddard Earth Observing System (GEOS) II GCM (Sud and Walker 1999, hereafter Part II).

2. Design of McRAS

A principal goal of this work is to improve the cloud processes in the 20-layer version of the GEOS II GCM employed for climate simulations. The GCM's moist convection scheme (RAS) was coupled to the new McRAS. However, both the stratiform and the boundary layer cloud schemes are also new and well merged into McRAS. For cloud microphysics, we have drawn heavily from the works of Sundqvist (1988), Sundqvist et al. (1989), Tiedtke (1993), and Del Genio et al. (1996). Consequently, McRAS has roughly the same level of cloud microphysics as in the references above. At least two other schemes, one by Cheng and Arakawa (1997) and the other by Fowler et al. (1996) have far more detailed cloud microphysics; we would like to adopt some of these design features into McRAS. The Zhao and Carr (1997) scheme in the National Centers for Environmental Prediction Meso Eta Model is another example of a pragmatic design that is based upon physical reasoning, some useful algorithms from Sundqvist et al. (1989), and the use of tuned empirical constants either for efficient calculations or for forecast improvement.

a. Governing equations

The governing prognostic equations of the dry static energy s, atmospheric water vapor q, and cloud water substance l, and cloud mass fraction f_c, in σ coordinates are

$$\frac{\partial \overline{p_s}\,\overline{s}}{\partial t} = -\nabla\cdot\overline{p_s}\,\overline{\mathbf{V}}\,\overline{s} - \frac{\partial}{\partial\sigma}\overline{p_s}\,\overline{\dot{\sigma}}\,\overline{s} + \overline{p_s}[L_e(\overline{C}-\overline{E}) + \overline{Q}_{\text{rad}}] - \nabla\cdot\overline{p_s\mathbf{V}'s'} - \frac{1}{\rho}\frac{\partial}{\partial\sigma}(\overline{\rho p_s\dot{\sigma}'s'}), \quad (1)$$

$$\frac{\partial \overline{p_s}\,\overline{q}}{\partial t} = -\nabla\cdot\overline{p_s}\,\overline{\mathbf{V}}\,\overline{q} - \frac{\partial}{\partial\sigma}\overline{p_s}\,\overline{\dot{\sigma}}\,\overline{q} - \overline{p_s}(\overline{C} - \overline{E}) - \nabla\cdot\overline{p_s\mathbf{V}'q'} - \frac{1}{\rho}\frac{\partial}{\partial\sigma}(\overline{\rho p_s\dot{\sigma}'q'}), \quad (2)$$

$$\frac{\partial \overline{p_s}\,\overline{l}}{\partial t} = -\nabla\cdot\overline{p_s}\,\overline{\mathbf{V}}\,\overline{l} - \frac{\partial}{\partial\sigma}\overline{p_s}\,\overline{\dot{\sigma}}\,\overline{l} + \overline{p_s}(\overline{C} - \overline{E}_l - \overline{G}_P) - \nabla\cdot\overline{p_s\mathbf{V}'l'} - \frac{1}{\rho}\frac{\partial}{\partial\sigma}(\overline{\rho p_s\dot{\sigma}'l'}), \quad (3)$$

$$\frac{\partial \overline{p_s}\,\overline{f_c}}{\partial t} = -\nabla\cdot\overline{p_s}\,\overline{\mathbf{V}}\,\overline{f_c} - \frac{\partial}{\partial\sigma}\overline{p_s}\,\overline{\dot{\sigma}}\,\overline{f_c} + \overline{p_s}(\overline{G}_{f_c} - \overline{D}_{f_c}) - \nabla\cdot\overline{p_s\mathbf{V}'f_c'} - \frac{1}{\rho}\frac{\partial}{\partial\sigma}(\overline{\rho p_s\dot{\sigma}'f_c'}). \quad (4)$$

Here, overbars denote grid-averaged variables and primes denote the subgrid-scale variations that produce turbulent eddies or the mesoscale circulation; $\mathbf{V}$ is the horizontal vector wind and p_s is the surface pressure. The local time rate of change of a conserved quantity [say, $p_S\phi$, which generically represents lhs of Eqs. (1)–(4)] equals the sum of the horizontal ($p_s\mathbf{V}\phi$) and the vertical ($p_s\dot{\sigma}\phi$) flux transport divergences plus the influence of physical interactions. The physical interactions consist of net radiative heating rate $\dot{Q}_{\text{rad}}$; condensation rate C, which is the sum of all condensation rates in the existing or newly formed clouds; evaporation rate E, which is the sum of the contributions from evaporation of cloud water/ice and falling precipitation, $E_l + E_p$; and the precipitation production rate G_P. Symbols G_{fc} and D_{fc} represent the generation and dissipation rates of cloud mass fraction. The constants C_p, L_e, and ρ are for the specific heat of air at constant pressure, latent heat of vaporization, and the density of ambient air, respectively. The turbulent flux transport divergences in the horizontal and vertical are represented by the last two terms in each of Eqs. (1)–(4). The vertical transport contains the sum of both Helfand and Lebraga (1988) turbulent transports and the cumulus flux transport of heat, moisture, cloud water substance, and cloud mass fraction. The dry static energy equation (1) can be transformed into the potential temperature tendency equation:

$$\frac{\partial \overline{p_s}\,\overline{\theta}}{\partial t} = -\nabla\cdot\overline{p_s}\,\overline{\mathbf{V}}\,\overline{\theta} - \frac{\partial}{\partial\sigma}\overline{p_s}\,\overline{\dot{\sigma}}\,\overline{\theta} + \frac{\overline{p_s}}{P}\left[\frac{L_e}{C_p}(\overline{C} - \overline{E}) + \frac{\overline{Q}_{\text{rad}}}{C_p}\right] - \nabla\cdot\overline{p_s\mathbf{V}'\theta'} - \frac{1}{\rho}\frac{\partial}{\partial\sigma}(\overline{\rho p_s\dot{\sigma}'\theta'}), \quad (5)$$

where $P = (p/p_0)^{\kappa}$; p and p_0 are the sigma-level and reference-level pressures, respectively; and $\kappa = R/C_p$; while the other symbols are as before.

In the GEOS II GCM, the horizontal turbulent flux divergences of the primary prognostic atmospheric fields (zonal and meridional winds, temperature, and humidity) are ignored. They only feature through the influence of the Shapiro filter S_f, whose primary role is to disperse the trapped 2-δx waves. On the other hand, turbulent flux divergences of cloud fraction and cloud water mixing ratios [Eqs. (3), (4)] cannot be handled by S_f because the cloud fields are highly discontinuous; nevertheless, it is important to allow diffusive mixing because the real atmosphere has significant flux transports through mesoscale circulation and turbulent diffusion. To address this problem, we use an explicit diffusion with diffusivity, $k_{\text{GD}} = 0.8 \times 10^5\ \text{m}^2\ \text{s}^{-1}$ for grid-scale diffusion and $k_{\text{CM}} = 0.5 \times 10^{-6}\ \text{s}^{-1}$ for subgrid-scale diffusion that dissipates the clouds.

The standard horizontal and vertical advection calculations are performed within the dynamical core of Suarez and Takacs (1995). The advection of all conserved variables is carried out in the same way as for q or θ, except that harmonic means are used to obtain cloud mass fraction f_c and cloud water substance mixing ratio l at the grid-cell boundaries. This virtually eliminates negative cloud water fields in advection; and, in rare situations (usually $<0.1\%$–0.5% of the time) if and when it happens, it is eliminated by borrowing the deficit amount from the surrounding grid cells in proportion to the cloud mass–weighted cloud water field of the donor grid cells. An alternative is to use the Lin and Rood (1996) advection scheme; however, that avenue has not been pursued seriously. For more details on the physical parameterizations of the GEOS GCM, see Takacs et al. (1994). With above modifications to Eqs. (2)–(5) and dropping overbars for brevity, the governing equations can be recast as follows:

$$\frac{\partial p_s\theta}{\partial t} = -\nabla\cdot p_s\mathbf{V}\theta - \frac{\partial}{\partial\sigma}\dot{\sigma}p_s\theta + \frac{p_s}{P}\left[\frac{L_e}{C_p}(C - E) + \frac{Q_{\text{rad}}}{C_p}\right] - S_\theta - \frac{1}{\rho}\frac{\partial}{\partial\sigma}(\rho p_s\dot{\sigma}'\theta'), \quad (6)$$

$$\frac{\partial p_s q}{\partial t} = -\nabla\cdot p_s\mathbf{V}q - \frac{\partial}{\partial\sigma}p_s\dot{\sigma}q - p_s(C - E) - S_q - \frac{1}{\rho}\frac{\partial}{\partial\sigma}(\rho p_s\dot{\sigma}'q'), \quad (7)$$

$$\frac{\partial p_s l}{\partial t} = -\nabla\cdot p_s\mathbf{V}l - \frac{\partial}{\partial\sigma}p_s\dot{\sigma}l + p_s(C - E_l - G_P) - \nabla\cdot p_s k\nabla l - \frac{1}{\rho}\frac{\partial}{\partial\sigma}(\rho p_s\dot{\sigma}'l'), \quad (8)$$

$$\frac{\partial p_s f_c}{\partial t} = -\nabla\cdot p_s\mathbf{V}f_c - \frac{\partial}{\partial\sigma}p_s\dot{\sigma}f_c + p_s(G_{f_c} - D_{f_c}) - \nabla\cdot p_s k\nabla f_c - \frac{1}{\rho}\frac{\partial}{\partial\sigma}(\rho p_s\dot{\sigma}'f_c'). \quad (9)$$

In the following sections, we shall discuss cloud water and ice parameterizations of McRAS that are intended to solve for the condensation, evaporation, cloud generation, cloud dissipation, and autoconversion of cloud

water/ice into precipitation with a fully consistent computation of cloud–radiation interactions.

b. Conceptual framework

McRAS explicitly caters to three types of clouds: convective, stratiform, and boundary layer. They are shown schematically in Fig. 1a. Accordingly, three cloud water source terms are introduced to compute condensation by large-scale, cumulus, and boundary layer clouds. Since the three cloud processes occur in parallel, the equations are solved in a Tiedtke (1993) style invoking simultaneous condensation and precipitation to solve for the net tendency.

Convective condensation and mass fluxes are produced by RAS due to Moorthi and Suarez (1992). We assume the cloud base can only exist at the top of a model layer in which the relative humidity is $\geq$90%; it can be any one of the lowest four layers above the surface layer. The relative humidity criteria merely ensure that the lifting condensation condition is attainable in convection either through turbulent eddies or subgrid-scale inhomogeneity of temperature and humidity. This limit helps to build convective available potential energy in the cloud sublayer before the onset of moist convection [see Emanuel et al. (1994) for a discussion of the trigger mechanism for moist convection]. Wang and Schlesinger (1995, 1999) demonstrate that neglect of this limit would weaken the Madden–Julian Oscillations. We also impose that the total energy required to maintain the convective mass flux (with precipitation loading and some momentum dissipation) must be provided by the thermal buoyancy available for cloud ascent. Critical cloud work function (CCWF), a concept first introduced into moist convection by Lord et al. (1982), represents the minimum amount of the buoyancy energy required to perform such ascent(s). Originally derived from the analysis of Marshall Island data by Lord (1978), the use of CCWF is also vital for a convection scheme. In our implementation, however, Lord's interpretation of CCWF was slightly modified by Sud et al. (1991) who introduced the so-called ''λ bounds'' to eliminate unrealistic solutions, which can happen, though quite infrequently. These limits use Simpson's (1971) experimental results.

The stratiform clouds emerge when the average relative humidity in a layer exceeds a statistically derived threshold value. However, the fractional clouds must blend with the newly formed and existing clouds to maintain the saturation vapor pressure both in advection and/or physical interactions. New stratiform clouds will form if the environmental relative humidity rises above the threshold value. Alternatively, if the relative humidity falls (rises), the clouds can evaporate (condense) the in-cloud water (vapor) to maintain the in-cloud saturation vapor pressure. The specific parameterization for this appears in section 2f. The key to the success of this parameterization is (i) a pragmatic choice of the prescribed value of threshold relative humidity as a function of height and (ii) a method for distributing the available increase in grid-scale relative humidity into cloud condensate, cloudiness increase, and increase in the ambient relative humidity.

The boundary layer (BL) clouds are produced by BL convection that almost always commences as dry convection. If rising BL eddies become saturated (as a consequence of adiabatic cooling) before detrainment at or below the level of inversion, the detraining BL eddy is cloudy and deposits excess water vapor as cloud condensate. We have adopted Tiedtke's construct in which surface fluxes and near-surface temperature gradients are employed to diagnose the BL mass and moisture fluxes that feed the BL clouds. This design can produce and maintain a cloudy boundary layer with drier air above and below—a typical scenario of countergradient BL fluxes. The cloud destruction mechanisms are the same for all clouds; for BL clouds, however, cloud-top entrainment and sinking within descending BL eddies are the primary mechanisms.

The convective clouds continue to generate precipitation during ascent and subsequent detrainment at the level of neutral buoyancy. However, they slowly transform into stratiform clouds (on the prescribed timescale of 1 h). The cloud fractions that get converted to the stratiform clouds naturally employ microphysical constants for the stratiform as opposed to convective clouds. In this way, the convective anvils transform into stratiform clouds. However, a proportionate amount of average-cloud fraction must sink and evaporate as a result of cloud-scale subsidence.

For all clouds, conversion of condensate into precipitation is carried out by a single algorithm due to Sundqvist (1988, 1993). The algorithm has internal adjustments for ambient temperature, Bergeron–Findeisen process of ice crystal growth, and collection by precipitating hydrometeors falling through the cloud. Full cloud microphysics remains active everywhere, including the cumulus towers and anvils. The momentum equation of an entraining and ascending convective cloud is integrated with full cloud microphysics to infer condensation and precipitation. The solution gives the updraft velocity, cross-sectional area, as well as the cloud ascent time per unit height. Of the total available precipitation, a fraction must be swept aloft with the updraft. For this calculation, Marshall–Palmer (1948) size distribution of hydrometeors, whose terminal velocity is available as a function of diameter from the experiments of Kinzer and Gunn (1951), is used. Finally, the detrained clouds merge into the existing cloud according to the schematic design discussed above.

The clouds in McRAS convect, advect, and diffuse both horizontally and vertically. The Suarez and Takacs (1995) dynamical core is adapted to perform the cloud advection while the numerical filters of the scheme are modified to carry out diffusion. As stated earlier, it was essential to use the harmonic mean for f_c and l in cal-

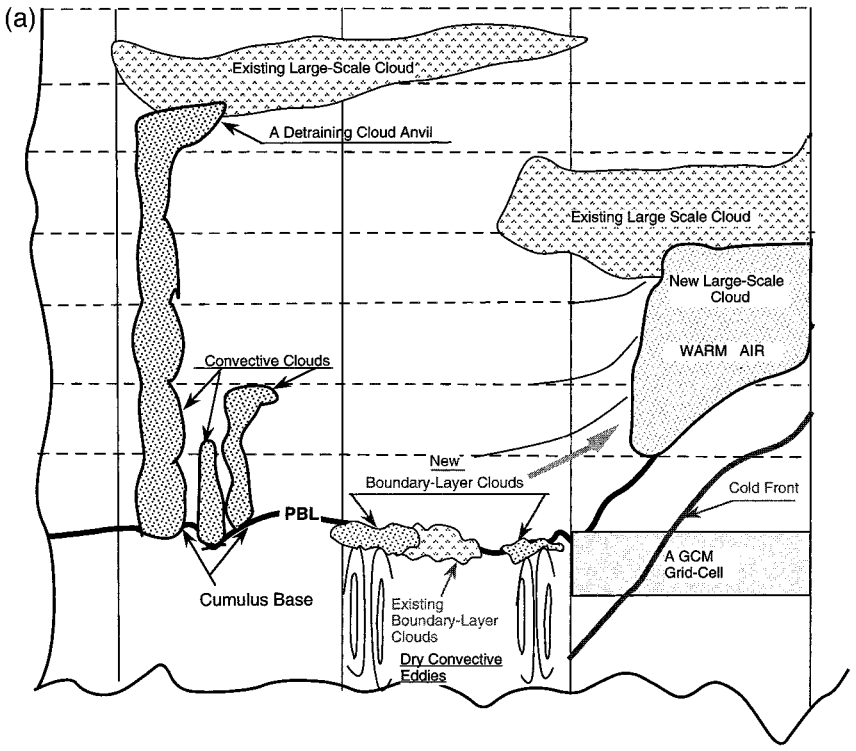

(b) Layer-by-Layer Cumulus Microphysics

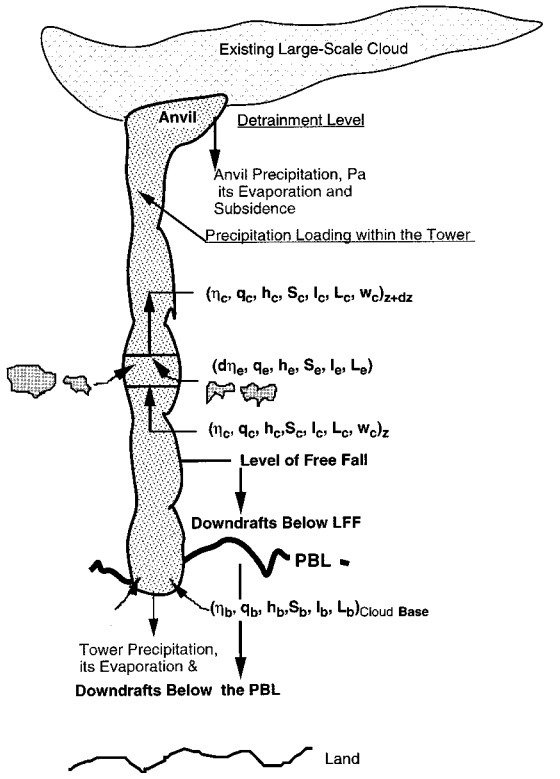

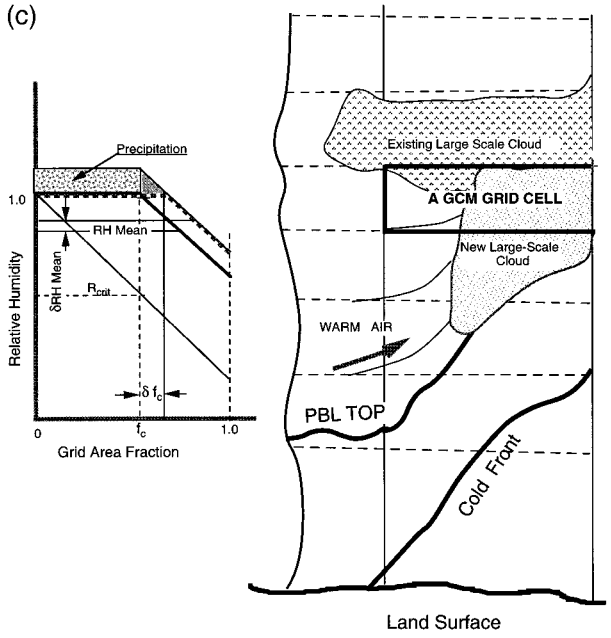

FIG. 1. Representation of emerging and merging convective, boundary layer, and large-scale clouds: (a) displayed side-by-side in the schematic, (b) layer-by-layer cloud microphysics of convective towers involving in-cloud condensation and autoconversion and collection, and (c) in-cloud condensation and growth of large-scale clouds.

culating the grid-cell boundary values. This assumption virtually eliminates the formation of negative fields. The alternative would be to neglect cloud advection as in Tiedtke (1993) and several other state-of-the-art schemes, but we submit that a somewhat subdued advection is better than no advection. The grid-scale moistening and cloudiness by cumulus-tower debris is a new feature of our design.

All clouds can be dissipated by buoyant mixing caused by cloud-top entrainment instability (CTEI) whose importance was originally identified by Randall (1980) and Deardorff (1980). Notwithstanding the controversy surrounding its role (Randall and Wielicki 1997), we argue that a physical process, howsoever innocuous, needs to be included in a model as long as it replicates the physical behavior of nature. It should only be ignored after simulation studies have unequivocally determined that the process remains consistently unimportant for all seasons and regions. We use a CTEI parameterization scheme of Del Genio et al. (1996) who have synthesized the existing algorithms of CTEI and its implications for a GCM using rational physical assumptions.

Sud and Walker (1993) combined the rain-evaporation parameterization and convective downdrafts to complement the Arakawa–Schubert (1974) moist-convective scheme. The basic momentum equation for cloud-scale downdrafts and updrafts remains the same. In downdrafts (updrafts) evaporative cooling (condensation heating) provides the negative (positive) buoyancy for descent (ascent). In this implementation, the precipitation falling inside cumulus towers (assumed saturated) undergoes no evaporation. However, the anvil precipitation, which falls through the unsaturated environment, undergoes evaporation. It can also entrain cloud water from the surroundings for instantaneous evaporation. At around 600 hPa, the criteria for free fall (where cooling due to evaporation of cloud water and from falling hydrometeors exceeds the adiabatic warming by subsidence) is satisfied and the downdrafts can ensue. In addition, the evaporation from tower precipitation below the cloud base could also satisfy free-fall criteria and produce downdrafts. Downdrafts naturally build dynamic pressure near the earth's surface, which enables detrainment to start above the surface, but our parameterization does not have such a provision; hence, all the downdrafts literally crash at the surface, displacing the near-surface air upward. Qian et al. (1998) have noted this to be a reasonable way of handling downdraft wakes produced in moist convection.

c. Convective condensation and precipitation

The RAS of Moorthi and Suarez (1992) provides the cumulus mass and energy fluxes involved in moist convection. The scheme solves for one cloud type at a time. The basic quantities required in the cloud microphysics are described in the following sections.

1) CUMULUS MASS FLUX DISTRIBUTION

The cloud mass flux η_z at height z above the cloud base is given by

$$\eta_z = \eta_B(1 + \lambda z) \tag{10}$$

and

$$\lambda = \frac{h_B - h_T^*}{\int_{\Delta z} (h_T^* - h_z)\, dz}, \tag{11}$$

where η_B is the cloud-base mass flux and λ is the entrainment parameter; h (h^*) is the actual (saturation) moist static energy; suffixes T and B are for top and bottom layers that contain the cumulus cloud; and Δz is the total vertical depth of the convective tower. Equation (10) represents the assumed linear growth of the cloud mass flux, while λ in (11) ensures that the cloud loses its buoyancy at detrainment. The basic criteria for (i) the emergence of a cloud type, (ii) the magnitude of cumulus base mass flux, and (iii) the requirement for a cloud to exceed the CCWF were formulated by Lord (1982) and remain essentially the same in RAS, the only difference being that RAS invokes a relaxation solution as opposed to an equilibration solution in Arakawa–Schubert (1974).

In this implementation, however, we not only diagnose the location of cloud base at the top of a layer whose relative humidity exceeds 90%, but we also disallow the cloud a second chance to detrain in the next level below if it fails the CCWF criteria for succeeding to reach its destination. In addition, we do not artificially mix the thermodynamic properties (temperature, humidity, and moist static energy) in all the layers below the cloud base for estimating the thermodynamic state of the cloud-base mass flux. On the contrary, we argue that turbulent mixing is the task of BL eddies and it must be performed by them on a physical basis. Our cumulus towers entrain the ambient air along with its fractional clouds. Consistently, the cloud mass fractions are also allowed to entrain, descend, and evaporate in the cumulus-induced subsidence and downdrafts. These idealizations were used in the current version of McRAS.

2) CONDENSATION–PRECIPITATION INTERACTION IN MOIST CONVECTION

A schematic representation of cloud microphysics in entraining convective towers is shown in Fig. 1b. The passage of clouds through a layer, L, is accompanied by (i) cloud mass flux entering from below (suffix b) and leaving at the top (suffix t) of a layer; (ii) in-cloud condensate, water vapor, and some swept-up precipitation; and (iii) the entrained airmass fraction $d\eta$, which contains water vapor q_e and cloud water substance l_e. The autoconversion of condensate into precipitation in

layer L, $\eta_t R_P l_t \Delta t_L$, is determined by the cloud microphysics. The parameter R_P is defined in (29) and the time taken by the cloud to traverse a layer L is Δt_L. Assuming it to be a quasi-steady-state process, the equations for cloud water substance and precipitation are as follows:

$$\eta_t[l + q^*(T_c, p)]_t = \eta_b[l + q^*(T_c, p)]_b + d\eta(q_e + l_e) - \eta_t R_P l_t \Delta t_L, \quad (12a)$$

and

$$\eta_t P_t + \mathrm{FP}_b = \eta_b P_b + \eta_t R_P l_t \Delta t_L + \mathrm{FP}_t, \quad (12b)$$

where $q^*(T_c, p)$ is the saturation water vapor mixing ratio at the cloud temperature T_c and pressure p. If (12a) leads to a negative in-cloud water content l_t, at exit, its value is made zero and the water vapor mixing ratio is adjusted to the subsaturation value that is consistent with cloud water conservation. Because all the precipitating hydrometeors do not fall right through, the fraction swept up by the updraft is a part of the precipitation budget in (12b). Here FP_t is the precipitation rising with the updraft, FP_b is the precipitation falling through, $R_P l_t$ is the rate of conversion of condensate into precipitation, and Δt_L is the time available for autoconversion in layer L. We again use Sundqvist (1988) for calculation of R_P, discussed in section 2f.

3) Determining Δt_L

For computing the time taken by the convective mass flux to travel through a layer, L, we use the cloud-scale momentum equation with implicit buoyancy and entrainment. The equation can be found in Simpson and Wiggert (1971). It represents vertical acceleration of a 1D cloud rising under the influence of thermal buoyancy B; cloud condensate and incloud precipitation loading, l_c and l_P; and parameterized frictional drag $K_d f(W)$. It is expressed by

$$W\frac{\partial W}{\partial z} = \frac{gB}{1+\gamma} - \frac{1}{\eta}\frac{\partial \eta}{\partial z}\frac{W^2}{2} - gl_c - gl_P - K_d f(W), \quad (13)$$

where $\gamma \equiv 1.5$ is the virtual mass coefficient, g is gravitational acceleration, and η is the mass flux.

We can recast (13) to introduce the effect of entrainment of ambient air with zero vertical velocity into the cloud. To simplify things, particularly to avoid W becoming very small at or near the detrainment level, and with the assumption that the tower precipitation stays within it, the effect of friction is included by use of a dissipation factor, α_f, that is applied to the buoyancy energy generated by the cloud. This was approximated from the structure of a typical velocity profile of the rising plumes discussed in Rogers and Yau (1989). The integral form of (13) is

$$\frac{1}{2}(\eta_t W_t^2 - \eta_b W_b^2) = \Delta z\left[g\frac{\overline{\Delta T}}{\overline{T}}\frac{}{1+\gamma} - g(l_c + l_P)\right]\overline{\eta}\alpha_f, \quad (14a)$$

and

$$\Delta t_L = \frac{2\Delta z_L}{(W_t + W_b)}. \quad (14b)$$

Here W_t and W_b are the cumulus updrafts at the top and bottom of the layer. The equation is integrated as an initial value problem and yields the vertical profile of temperature and velocity. An initial rise rate of 1.0 m s^{-1} at the cloud base is assumed; however, its initial magnitude is unimportant as inferred by Simpson and Wiggert (1971). The time Δt_L is determined from (14b) and is used for conversion of incloud condensate into precipitation.

4) Determining l_c and l_P

Cloud condensate loading l_c is the average cloud condensate amount in the layer. In our scheme, only l_{ct} and l_{cb} are available. Therefore, we use a mass-weighted average to represent l_c. Its minimum value has to be zero from considerations for (12a).

For precipitation loading, the precipitation falling through the tower is added to the precipitation swept up from below and the precipitation generated by autoconversion of condensate per unit cloud-base mass flux. The total mass flux of precipitated hydrometeors is

$$\eta_t P_t + \mathrm{FP}_b = P_{\mathrm{avail}}.$$

Out of P_{avail}, the fraction carried aloft is the part whose terminal velocity is less than the updraft velocity. Thus small droplets in the precipitation spectrum continue to rise even while falling relative to the cumulus updraft. We estimate the falling mass fraction of hydrometeors is P_{avail} multiplied by a function of the ratio of updraft velocity, W_{up}, in the tower and mean terminal velocity of hydrometeors, V_T, inside the tower by

$$P_{\mathrm{fall}} = P_{\mathrm{avail}} \exp(-W_{\mathrm{up}}/V_T). \quad (15)$$

From P_{fall}, we can now calculate the precipitation intensity P_i as follows:

$$P_i = \frac{P_{\mathrm{fall}}}{a_c} = \frac{P_{\mathrm{fall}}\rho_{\mathrm{air}} W_{\mathrm{up}}}{\eta_z m_{\mathrm{cb}}}, \quad (16)$$

where a_c is the fractional area of the convective tower, η_z is from (10), ρ_{air} is the density of air, and m_{cb} is the cloud-base mass flux. The Marshall–Palmer (1948) spectrum of drop-size distribution of precipitation, at any height, z, taken from Kessler (1969, p. 28), is

$$V_T = 38.3 N_0^{-1/8} M^{1/8} \exp(\kappa z/2). \quad (17a)$$

The corresponding precipitating water-substance mixing ratio M is

$$P_i = 138 N_0^{-1/8} M^{9/8}. \quad (17b)$$

From (17b) we get M, and then the precipitation loading l_P is simply

$$l_p = M/\rho. \quad (17c)$$

d. Stratiform condensation

The stratiform clouds are formed by supersaturation produced by either diabatic cooling or the large-scale motion fields causing adiabatic cooling. Large-scale motion enables either the incoming warm moist air to ride over the colder and drier near-surface air (warm front) or cause the incoming cold air to undercut the near-surface warm moist air (cold front). In both cases, moist air is displaced upward causing adiabatic cooling and condensation. In our scheme, stratiform condensation represents supersaturation of a fraction of a grid cell in which subgrid-scale temperature and water vapor distribution lead to supersaturation. At all times, the relative humidity inside the cloudy fraction of the grid cell must be maintained at 100%. Any excess (deficit) water vapor in the cloud generates (consumes) cloud water. However, subgrid-scale inhomogeneity in temperature and humidity fields can cause condensation to occur well before the grid-mean relative humidity reaches the saturation value. This is accomplished by assuming a linear relationship between relative humidity and cloud mass fraction. The slope of this distribution is determined by the critical relative humidity R_{crit}, a threshold value at which the clouds begin to emerge and in-cloud condensation ensues, as shown in Fig. 1c. The design yields a cloudiness fraction, f_c, as a function of mean relative humidity $\overline{R}$ and R_{crit}. The relationship derived from the above assumptions is identical to that of Sundqvist (1988):

$$f_c = 1 - \sqrt{\frac{1 - \overline{R}}{1 - R_{\text{crit}}}}. \quad (18)$$

Mocko and Cotton (1995) show that the Sundqvist scheme does a superior job on fractional cloudiness in a mesoscale stratiform situation. Its derivative with $\overline{R}$ gives the rate of change of cloudiness with change in grid-averaged relative humidity:

$$\frac{\partial f_c}{\partial \overline{R}} = \frac{1}{2}\sqrt{\frac{1}{(1 - R_{\text{crit}})(1 - \overline{R})}}. \quad (19)$$

For stratiform clouds, the cloud production rate will be determined by R_{crit} and $\overline{R}$. On the other hand, if the cloud is the end product of convective debris, it is not expected to have any relationship with grid-scale relative humidity. In our design, the relative humidity–cloudiness relationship is physical for generating new stratiform clouds but is inconsequential for existing clouds that may be produced by cumulus or BL convection or brought in by advective diffusion. Our design features can handle such cloud scenarios.

In the atmosphere, we encounter three stratiform cloudiness change scenarios: one is the condensation or evaporation in an advecting cloud; another is the condensation within a growing cloud because its grid-mean relative humidity $\overline{R}$ becomes higher than the minimum necessary to maintain the existing stratiform cloudiness; and the third is cloud water generation or evaporation within a fully cloudy region of the grid cell. These are carried out sequentially with one or more of the above cloud processes, as necessary. Each condensation or evaporation event naturally affects the specific humidity and temperature of the succeeding stratiform process. A typical scenario is shown in Fig. 1c; any relative humidity higher than that necessary to support the existing cloudiness causes in-cloud condensation as well as increases the cloud fraction. Alternatively, warming or decreasing in-cloud humidity would evaporate the cloud water without decreasing the cloudiness. The cloudiness only reduces by cloud munching, that is, diffusive mixing of cloud and ambient air, and/or CTEI. These processes are discussed below.

1) CONDENSATION–EVAPORATION IN AN EXISTING CLOUD

This would be a straightforward calculation if the clouds were nonadvecting. However, to determine in-cloud specific humidity following an advecting cloud, we advect both the cloud mass fraction–weighted saturation humidity $f_c^{(n)} q^{*(n)}$ and cloud fraction $f_c^{(n)}$ separately (both of which are conserved except for $f_c > 1$) and then the saturation humidity $\tilde{q}^{*(n+1)}$ of the aggregated cloud becomes

$$\tilde{q}^{*(n+1)} = \frac{\{f_c^{(n)} q^{*(n)} + \Delta_{\text{adv}}[f_c^{(n)} q^{*(n)}]\}}{f_c^{(n)} + \Delta_{\text{adv}}\{f_c^{(n)}\}}. \quad (20)$$

The in-cloud condensation or evaporation at the next time step $(n + 1)$ will be $\tilde{q}^{*(n+1)}$ minus q^* where q^* is based on the new temperature and pressure. However, the process must affect the grid-cell temperature due to buoyant mixing and turbulence produced by the cloud. This yields

$$\frac{dl}{dt} = \frac{1}{\tau}\frac{[\tilde{q}^{*(n+1)} - q^*(T^{n+1}, p^{n+1})] f_c^{(n+1)}}{\left[1 + \dfrac{L}{c_p} f_c^{(n+1)} q^*(T^{n+1}, p^{n+1}) \dfrac{b}{T^2}\right]}. \quad (21a)$$

Using the standard form of q^* as a function of temperature and pressure,

$$q^* = \frac{\exp(a - b/T)}{p}, \quad \text{gives } \frac{\partial q^*}{\partial T} = q^* \frac{b}{T^2}. \quad (21b)$$

Equation (21a) takes into account the effect of condensation (evaporation) heating (cooling) in an implicit way and distributes it into the entire grid cell. It assumes that cloud mass is conserved in advection while its temperature or pressure is not. The heating or cooling occurs initially in the cloud, but it is as-

sumed to get uniformly distributed. In (21), τ is the physics time step. Naturally, we must limit maximum in-cloud evaporation to the available cloud water. If and when it happens, all the cloud condensate evaporates and the cloud vanishes [a design concept adopted from Tiedtke (1993)].

2) CONDENSATION WITH INCREASING CLOUD COVER

This calculation is invoked when the grid-scale relative humidity $\overline{R}$ is larger than the humidity required $R_{\rm rqd}$ for supporting an existing cloud fraction from (18). It implies

$$\overline{q} > q_{\rm rqd}, \tag{22a}$$

where

$$q_{\rm rqd} = R_{\rm rqd} q^*(T, p), \tag{22b}$$

and

$$R_{\rm rqd} = [1 - (1 - f^c)^2(1 - R_{\rm crit})]. \tag{22c}$$

As can be seen in Fig. 1c, increasing the relative humidity of a layer by physical processes can increase the cloud fraction as well as produce additional in-cloud condensation. It is a two-part process: one gives new in-cloud condensation or evaporation accompanied by cloudiness increase (not decrease) and the other makes the relative humidity of clear air rise. The excess relative humidity $\overline{R} - R_{\rm rqd}$ is assumed to be uniformly distributed in the grid cell. Within the cloud, it becomes condensate, $(\overline{R} - R_{\rm rqd}) f_c$, while for the clear air it is just higher relative humidity:

$$\delta R_c = (1 - f_c)(\overline{R} - R_{\rm rqd}), \tag{23a}$$

However, following (19) δR_c must be accompanied by cloud fraction increase, δf_c, which gives

$$\delta f_c = \left[\frac{1}{2}\sqrt{\frac{1}{(1 - R_{\rm crit})(1 - \overline{R})}}\right]\delta R_c. \tag{23b}$$

Substituting from (23a) and solving, we get

$$\delta f_c = \frac{\overline{R} - R_{\rm rqd}}{2(1 - R_{\rm crit})}. \tag{23c}$$

The corresponding production of cloud condensate, using implicit adjustment as in (21), gives

$$\frac{dl}{dt} = \frac{1}{\tau}\frac{(q^{n+1} - q^{n+1}_{\rm rqd})C_R}{\left(1 + \dfrac{L}{c_p} C_R q^{n+1}_{\rm rqd}\dfrac{b}{T^2}\right)}, \tag{24}$$

where $C_R = f^n_c + 0.5\delta f_c$; $q_{\rm rqd}$ is from (22c), and the implicit calculation accounts for temperature increase due to condensation.

3) CONDENSATION IN A HOMOGENEOUS (FULLY CLOUDY OR CLEAR) ENVIRONMENT

For this case, the adiabatic saturation humidity of the entire layer is the most important quantity because it determines the net condensate production and temperature change through condensation heating. We solve this (and maximum possible evaporation of falling precipitation in downdrafts) by an efficient ''energy method.'' Realizing that, at any given atmospheric pressure, there can be one and only one T^* and q^* for any given equivalent temperature (sum of sensible and latent heat for the actual and adiabatically saturated environment), $T_{\rm enr}$, we proceed as follows:

$$T_{\rm enr} = T + \frac{L}{c_p} q \tag{25a}$$

$$= T^* + \frac{L}{c_p} q^*(T^*, p), \tag{25b}$$

giving

$$T^* = T^*(T_{\rm enr}, p). \tag{26a}$$

Hence, T^* is a unique function of $T_{\rm enr}$ and p, provided the saturation is achieved by adiabatic evaporation or condensation, which clouds naturally do. We have created a precalculated bilinear table look up at 2°C and 100-hPa intervals, which is used to determine the first guess value of T^*; from T^*, we get $q^* = q^*(T^*, p)$. We then calculate the moist static energy error δT_ε:

$$\delta T_\varepsilon = T_{\rm enr} - (T^* + L/c_p q^*). \tag{26b}$$

The moist static energy error δT_ε can be used to solve for an energy-conserving estimate of $q^*_{\rm as}$ as follows:

$$q^*_{\rm as} = q^*\left(1 + \frac{b/T^2 \delta T_\varepsilon}{1 + (L/c_p)(b/T^2 q^*)}\right). \tag{26c}$$

Any excess (deficit) water vapor amount is tied to $q^*_{\rm as}$ for both cloud water and/or rain evaporation within the grid cell.

e. Boundary layer clouds

The BL cloud scheme in McRAS is relatively straightforward. The BL clouds are formed by the turbulent eddies carrying water vapor into the highest detraining levels below the inversion. The turbulent eddies are assumed to carry the surface fluxes (sensible heating and evapotranspiration) into the mixed layer as well as the detrainment level. These fluxes increase the virtual temperature and lead to transport of mass and moisture from the surface to the detraining layers. We estimate the circulating eddy mass flux $M_{\rm eddy}$ from

$$E_S = M_{\rm eddy}(q_{\rm up} - q_{\rm dn}), \tag{27}$$

where E_S is the surface evaporation rate in a boundary layer, and $q_{\rm up}$ and $q_{\rm dn}$ are upwelling and downwelling

TABLE 1. Some common constants.

Symbols(s)	Units	Stratiform clouds values	Convective/BL clouds values	BL clouds values
C_0^*	(s^{-1})	3.33×10^{-3}	10^{-3}	10^{-3}
C_1	(s kg^{-1})	100.	100.	
C_2	($°C^{-1}$)$^{0.5}$	0.65	0.65	
l_{crit}^*	(kg m^{-3})	0.3×10^{-3}	10^{-3}	
l_{min}	(kg m^{-3})	0.1×10^{-3}	0.1×10^{-3}	
κ_{CM}	(s^{-1})	0.5×10^{-6}	0.5×10^{-6}	0.5×10^{-6}
κ_{GD}	(m^2 s^{-1})	0.8×10^5	0.8×10^5	0.8×10^5
R_{crit}	(frac.)		Slingo (1987) curve with 80% min	None
γ	Dimensionless		1.5	
α_f	Dimensionless		0.666	
$c_{min}(c_{max})$	Dimensionless	0.23 (0.7)	0.23 (0.7)	
Cahalan correction	Dimensionless	0.6065	0.38	0.6065
BL cloud mass Fract	Dimensionless			0.25
Bl inversion $\frac{\Delta h}{c_p \Delta p}$	(°C hPa^{-1})			0.25

specific humidity fields within the eddy. Naturally, because the boundary layer is well mixed, the detrainment of heat and moisture into the mixed regime of the BL must be uniform. We assume only a fraction, f_M, of this flux lands at the inversion. Although f_M can vary anywhere from 0% to 100%, Deardorff (1976) arguments suggest a value close to 50%. We have arbitrarily chosen $f_M = 25\%$ in recognition of the fact that there is turbulent diffusion of T and q acting in parallel, which represent turbulent eddies (Helfand and Lebraga 1988). This value is in good agreement with Betts estimates for top of the boundary layer (TBL) fluxes for First International Land Surface Satellite Climatology Project Field Experiment observations (A. K. Betts 1996, personal communication). With the above assumption, we infer the turbulent eddy mass flux to be

$$M_{\text{eddy}} = \frac{f_M E_s}{q_s - (q_t + l_t)}. \tag{28}$$

The turbulent eddies in the BL detrain into or near the inversion layer, which is diagnosed from the buoyant stability of the layer, $(\Delta h/c_p)\, dp$ (Table 1). The test is performed for the bottom six layers (representing roughly 25% mass of the column atmosphere) starting from the surface layer and, if this criteria is not fulfilled, BL clouds do not form. The PBL eddies would be supersaturated if $q^*(T_t, p_t)$ is less than q_s. The difference $q_s - q^*(T_t, p_t)$ would be the BL cloud water loading, l_c. The BL clouds also merge with the existing clouds and can precipitate like other clouds, but only after l_c becomes larger than l_{min}, the minimum in-cloud water substance required to generate precipitation (Table 1). The BL clouds would become persistent if their production is in equilibrium with their removal by CTEI or other cloud-dissipating processes.

f. Microphysics of precipitation

The precipitation rate G_P according to Sundqvist (1988) is a function of specific cloud water substance l_c and autoconversion parameters l_{crit}, and a time constant C_0. It is related to precipitation formation rate R_P through l_c. The equation is

$$G_P = \frac{l_c f_c}{C_0}\left\{1 - \exp - \left(\frac{l_c}{l_{\text{crit}}}\right)^2\right\} = l_c R_P. \tag{29}$$

Several scientists (e.g., LeTreut and Li 1988; Tiedtke 1993; Del Genio et al. 1996; Zhao and Carr 1997) have used this equation, but in most applications there are some modifications. For example, Tiedtke (1993) uses a different formulation for high clouds with precipitating ice crystals; Del Genio et al. (1996) alter the exponent and include the influence of collection of cloud water separately. In the formulation here, we have kept Sundqvist (1988) in its original form, but we plan to modify it with systematic evaluation experiments in SCMs using observational data such as ARM-CART (Zhang and Lin 1997). The Sundqvist formulation includes modification of the basic constants C_0^* and l_{crit}^* with three additional parameters to arrive at the operational value of C_0 and l_{crit} for the cloud as follows:

$$C_0 = C_0^* F_1 F_2 F_{\text{co}}, \tag{30a}$$

and

$$l_{\text{crit}} = l_{\text{crit}}^*/F_1 F_2 F_{lc}. \tag{30b}$$

The factors F_1, F_2, and F_{co}/F_{lc} are similar to Sundqvist et al. (1989), but C_2 is modified to achieve a smooth transition from low to high clouds. Specifically,

$$F_1 = 1.0 + C_1 \tilde{P}^{0.5} \quad \text{with } C_1 \equiv 100, \tag{31}$$

where $\tilde{P}$ is the intensity of precipitation (kg sec^{-1}),

$$F_2 = 1.0 + C_2(268 - T)^{0.5} \quad \text{with } C_2 \equiv 0.65. \tag{32}$$

In (32), temperature T must remain within 253 to 268 K, where ice crystals and water droplets coexist leading to increased growth of precipitation particles by the Bergeron–Findeisen process. The clouds at these temperature produce condensation in the form of snow or ice crystals.

The third factor F_3 is for precipitation production in the high cloud at temperatures below 253 K. It has separate forms for conversion timescale F_{co} and critical cloud water substance F_{cl}. The equation for F_{co} is the same as in Sundqvist except that it is made to vary linearly from the F_2 value at 253 K to its maximum value of 5.0 at 233 K. The interpolation relation is

$$F_{co} = a_c + b_c(T_c - T), \tag{33}$$

where a_c and b_c are the intercept and slope of a straight line passing through two points, and $T_c = 253.0$ K, with $T = \max(T, 233.0)$.

For l_{crit} we invoke the original Sundqvist (1988) relation in which

$$F_3 = F_{cl}^{-1}, \tag{34a}$$

$$F_{cl} = 0.15\left(1.07 \pm \frac{y}{1 + y}\right), \tag{34b}$$

Here, y is a function of temperature T and is given by

$$y = x\left(1 + x + \frac{4}{3}x^2\right), \quad \text{and} \tag{35a}$$

$$x = \left|\frac{T - 233}{17}\right|. \tag{35b}$$

For cloud temperatures below 253 K, F_{co} replaces F_2. To maintain the simultaneity of condensation and precipitation production, R_P from (29) is used to solve the simple differential equation as in Tiedtke [1993, Eq. (36)]. That method gives satisfactory results for cloud and precipitation production with generation and dissipation terms. A comparison of the product, F2 × F3, resulting from the original constants of Sundqvist (1989) vis-à-vis the modified constants $C_2 \equiv 0.650$ is shown in Fig. 2a. Evidently, the new constant eliminates the discontinuity at 253 K, which is desirable for GCM parameterizations.

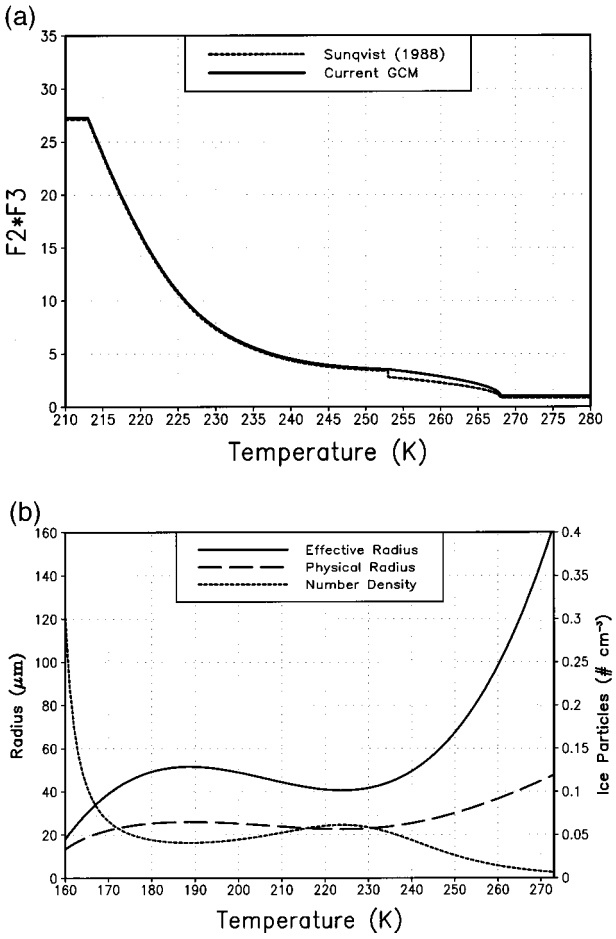

FIG. 2. (a) Distribution of F2 × F3 as a function of temperature for Sundqvist (1988) formulas (dashed curve) and modified equations with $C_2 = 0.65$ (solid curve). (b) Calculation of effective and physical radius for ice clouds as a function of temperature. For a visual picture of number density distribution of cloud-ice particles, let us take $l_{ice} = 5.0$ mg kg^{-1}.

g. Cloud dissipation

Clouds can be affected by advective subsidence and diffusion or by radiative heating. These effects are discussed in sections 2h and 2i, respectively. The other cloud dissipation mechanisms are (a) cloud top entrainment instability and (b) diffusive mixing of the dry and cloudy air masses within the grid cell. These parameterizations are discussed below.

1) CLOUD-TOP ENTRAINMENT INSTABILITY

Despite the controversy about the role of CTEI in influencing the stratus cloud decks, we contend that the CTEI mechanism is not only real but is well simulated in some cloud-resolving models (e.g., Witting 1995); therefore, its representation into GCMs is very worthwhile. We have implemented the Del Genio et al. (1996) algorithm, which is based on the present-day understanding of the behavior of cloud mixing with clear air aloft under the influence of CTEI. For completeness, we summarize the Del Genio parameterization here. First, a parameter, c, is calculated:

$$c = \frac{\Delta h}{L\Delta(q_c + l_c)}. \tag{36}$$

Here h is the moist static energy, and q_c and l_c are the in-cloud water vapor and condensate mixing ratios. The differencing operator Δ is for differences between the cloudy layer and the clear air above. Del Genio et al. (1996) constructed the following interpolation formula for CTEI-generated mass exchange. A function, $\psi(c)$, is introduced:

$$\psi(c) = 2.0 \times 10^{-4}\left(\frac{c - c_{min}}{c_{max} - c_{min}}\right)^5. \tag{37}$$

In (37), $c_{\min}$ is estimated to be 0.23 from observation; this is the threshold at which onset of CTEI ensues (observations); an upper limit of c is $c_{\max} = 0.7$. It gives the e-folding cloud dissipation timescale represented by $\tau^{-1} = 2.0 \times 10^{-4}$ s^{-1}. The specific value of τ is also estimated from observational data. When c is below $c_{\min}$, $\psi(c)$ is negative and is set equal to zero; that is, CTEI does not happen. For $c > c_{\min}$, $\psi(c)$ is calculated, but its maximum value is 2.0×10^{-4} s^{-1}. For nonzero $\psi(c)$, a ζ fraction of the cloud mass is exchanged with the cloud-free air above, where ζ is estimated from

$$\zeta = 1 - \exp[-\psi(c)\Delta t]. \tag{38}$$

The rising (sinking) cloudy (clear) air masses are mixed into the local ambient (cloudy) environment conserving the moist static energy and total water content. More details of the basis and the specific choice of cloud dissipation timescales are available in the original paper of Del Genio et al. (1996).

2) Diffusive mixing, also called "cloud munching"

Our cloud-munching calculation assumes an eddy mixing between the moist in-cloud air and the clear cloud-free air of the grid cell. We follow the Tiedtke (1993) scheme of turbulent eddy mixing produced by evaporation driven by saturation-specific humidity deficit:

$$\frac{dE_{\text{diff}}}{dt} = f_c A_c \kappa[q^*(T_c, p) - q], \tag{39}$$

where E_{diff} is the evaporation of cloud water or ice by diffusion of the surrounding clear air, k is the diffusivity and is equal to 0.5×10^{-6} s^{-1}, and $A_c = 2\sqrt{3}$ is a factor for relationship between the surface area of the cloud and its mass fraction f_c. The cloud munching only occurs if f_c is larger than the value that can be supported by the relative humidity–cloudiness relationship expressed in (18). Cloud munching is likely to be strong in convective episodes because convection can detrain clouds in all environments regardless of the local specific humidity. The cloud-munching calculation only aims at estimating the amount of cloud water evaporated. Correspondingly, the reduction in cloud fraction and cloud water substance is given by

$$\frac{df_c}{dt} = \frac{1}{l_c}\left(\frac{dE_{\text{diff}}}{dt}\right), \tag{40a}$$

$$\frac{dl}{dt} = l_c \frac{df_c}{dt}. \tag{40b}$$

Naturally, evaporation of a fraction of cloud has its consequences on the temperature and water vapor content of the entire layer, but those are included easily through heat and moisture conservation.

3) Cloud production and dissipation

Figure 1a shows schematically three major sources of in-cloud condensation. In this design, the growth rate of clouds is the sum of new cloud production rate, G_{f_c}, multiplied by the clear-sky fraction (to account for its partial merger into an existing cloud), while the dissipation rate of the cloud, D_{f_c}, is caused by cloud water evaporation as a consequence of warming or munching by diffusive mixing of dry air and CTEI. Both of these are proportional to the cloud fraction itself. This leads to the following differential equation:

$$\frac{df_c}{dt} = f_c D_{f_c} + (1 - f_c) G_{f_c}. \tag{41}$$

Equation (41) is an ordinary differential equation if G_{f_c} and D_{f_c} are assumed invariant during the time step; its solution is straightforward and is given in Tiedtke (1993). A more rigorous way of solving the complete system of equations, for a three-way interaction between cloud water, cloud ice, and precipitation, is provided in Fowler et al. (1996).

h. Cloud advection and diffusion

Cloud fields vary between zero and a finite value in short space and time intervals. Consequently, cloud advection has been recognized to be a difficult problem because cloud fields are exceptionally discontinuous while almost all advection schemes leave a 2-δx structure as unresolvable. For T and q fields, filters are used to disperse the 2-δx structures, but when the key features of cloud field mingles with the 2-δx structures, filters will not work. Therefore, one must look for other ways of handling cloud fields. This is done by invoking grid-scale diffusion. For the present, diffusivity $k = 0.8 \times 10^5$ m^2 s^{-1} is assumed. This gives a diffusion timescale of 20 days as opposed to an advection timescale of the order of a day or less. This value is low to keep the diffusion to a minimum. Second, advection out of a grid cell with zero cloud field will generate a negative value of the field; therefore, we must find ways to suppress this tendency. Harmonic interpolation for the grid-cell boundary values of cloud fields eliminates this problem for the C-grid environment. Obviously, this method has drawbacks because it forestalls the movement of a strong structure in the field; but on the positive side, it does not produce negative fields as often. Indeed, the diffusion is invoked to dismantle strong grid-scale cloud structures. Without harmonic interpolation, we cannot advect a discontinuous field and we contend that a sluggish advection is better than no advection, particularly for semipermanent features such as ITCZ or the South Pacific convergence zone, which, in the absence of advection, are likely to produce overly strong cloud-radiative forcing.

Cloud mass fraction and total cloud water substance are advected by treating them as passive quantities. The

Suarez and Takacs (1995) scheme guarantees conservation, which is particularly important for the cloud water substance. Since there is no advective coupling between cloud water and cloud mass fraction, we can encounter situations in which cloud mass fraction becomes zero while cloud water substance does not, or vice versa. Both situations are handled adequately in McRAS. Former occurrence leads to instantaneous removal of cloud water by conversion to precipitation while the latter leads to instantaneous disappearance of the cloud itself. These scenarios are discussed in Tiedtke (1993), although his implementation in the European Centre for Medium-Range Weather Forecasts model did not include explicit cloud advection. Since clear (cloudy) days are often associated with subsiding (rising) motion, cloud advection in the vertical is very important. Having realized this, we undertook the task of parameterizing cloud advection and produced the current scheme that advects clouds in three dimensions. In Part II, we shall show some evidence of a significant influence of cloud advection on clouds and cloud-radiative forcing.

i. Cloud-radiation interaction

Uncertainties in cloud-radiative forcing are among the prime causes of contention among scientists on the usefulness of climate change scenarios predicted with GCMs. McRAS is designed to perform cloud-radiative forcing in an interactive and dynamical framework. McRAS also provides cloud mass fraction, cloud droplet and/or cloud ice crystal path lengths, and effective radii of cloud particles. The in-cloud water and ice mass fractions are diagnosed from Eq. (12) of Del Genio et al. (1996). To be consistent, we use Del Genio's approximations for the number density of cloud particles over land and ocean. One modification involves a calculation for the equivalent plane parallel optical thickness using Cahalan (1994) correction to account for the inhomogeneity in the cloud water. A second modification was included at the time of GCM implementation in the GEOS II GCM. In this, the number density and effective radius of ice clouds is a function of temperature following Lohmann et al. (1999). The structure of this distribution for an arbitrary in-cloud water substance is shown in Fig. 2b.

There are four bands in the shortwave (Chou et al. 1998) and nine bands in the longwave (Chou et al. 1999) radiation. For each band, we require the optical thickness τ, single scattering albedo ω, and asymmetry factor g for the clouds (see Table 2 for optical parameters). The linearized approximation to the precise radiative transfer equations yields

$$\tau_i^\lambda = W_i\left(a_i^\lambda + \frac{b_i^\lambda}{r_{e_i}}\right), \tag{42}$$

$$\omega_i^\lambda = c_i^\lambda + d_i^\lambda r_{e_i}, \tag{43}$$

$$g_i^\lambda = e_i^\lambda + f_i^\lambda r_{e_i}, \tag{44}$$

TABLE 2. Parameters for radiation.

Parameter Symbol(s)	Units	Values	
		Land	Ocean
Effective rad., r_e (water)	(10^{-6} m)	7.0	10.0
Number Density, N (water)	(cm^{-3})	170.0	60.0
Effective rad., r_e (ice)*	(10^{-6} m)	25.0	25.0
Number Density, N (ice)*	(cm^{-3})	0.06	0.06

* Also from Ou and Liou (1995) and Moss et al. (1996). See Fig. 2b

where suffix λ represents the spectral band and index, $i = 1$ or 2 for in-cloud ice or water. The constants a_i^λ, $b_i^\lambda, \ldots, f_i^\lambda$ are regression coefficients derived from Mie scattering calculations of Tsay et al. (1989) for water droplets and ray-tracing techniques of Fu (1996) for ice crystals using high spectral resolution data. Here W_i is the water/ice path in a layer and r_{ei} is the effective size of the ensemble. The actual values of these constants are given in Chou and Suarez (1994).

The optical thickness, single scattering albedo, and asymmetry factor for in-cloud water and ice mixtures employ a weighted summation, as follows:

$$\tau^\lambda = \tau_{\text{ice}}^\lambda + \tau_{\text{water}}^\lambda, \tag{45}$$

$$\omega^\lambda = \frac{\tau_{\text{ice}}^\lambda \omega_{\text{ice}}^\lambda + \tau_{\text{water}}^\lambda \omega_{\text{water}}^\lambda}{\tau_{\text{ice}}^\lambda + \tau_{\text{water}}^\lambda}, \tag{46}$$

$$g^\lambda = \frac{\tau_{\text{ice}}^\lambda \omega_{\text{ice}}^\lambda g_{\text{ice}} + \tau_{\text{water}}^\lambda \omega_{\text{water}}^\lambda g_{\text{water}}}{\tau_{\text{ice}}^\lambda \omega_{\text{ice}}^\lambda + \tau_{\text{water}}^\lambda \omega_{\text{water}}^\lambda}. \tag{47}$$

The clouds in any atmospheric column are divided into three height groups. Within each group, the clouds are assumed to be maximally overlapped while among the groups; the clouds are assumed to be randomly overlapped. To calculate the optical thickness of different clouds within the group, smaller clouds are smeared to the size of the largest cloud of the group; this entails adjustment of the in-cloud optical thickness for each cloud except the largest. The specific calculation differs somewhat for shortwave and longwave radiation as follows.

For shortwave radiation, the optical thickness of the smeared cloud, $\tilde{\tau}$, is the product of τ and χ, where χ is precalculated from detailed radiative transfer calculations. Dropping prefixes and suffixes for brevity, the functional form of the relation is

$$\tilde{\tau} = \tau\chi(f_c, \mu_0, \tau), \tag{48}$$

where χ is a function of cloud fraction f_c with respect to group, cosine of solar zenith angle μ_0, and the optical thickness τ.

For longwave radiation, the effect of backscattering is folded into the emission of an atmospheric layer, and absorption between the levels is calculated by scaling the cloud optical thickness appropriately. With these approximations, the longwave radiative transfer equations for cloudy atmosphere are identical to that for the

clear atmosphere. The smeared optical length uses the following functional form:

$$\tilde{\tau} = \tau[1 - \omega h(g)]. \quad (49)$$

Here also, $\tilde{\tau}$ is equal to τ times a factor, which depends upon the single scattering albedo ω and a forward scattering function h, which depends upon the asymmetry factor g. Further details of these calculations are available in Chou et al. (1998, 1999).

3. SCM simulation with McRAS

The original GATE Phase III data is available in the discretized form at 3-h time intervals and 25-hPa vertical intervals. We reduced the data to the same 17 sigma levels that correspond to the 17-layer version of the GEOS I GCM (hereafter simply GATE data). The data contain surface fluxes of heat and moisture (based on estimate of observations) as well as observed horizontal flux divergences of heat, moisture, and mass for the column. In addition, the vertical motion fields are available and those are used to compute the prescribed adiabatic cooling of the GATE column. The data have been extensively used for testing cloud parameterizations in an SCM environment (Lord 1982; Krishnamurti et al. 1983; Kuo and Anthes 1984; Betts and Miller 1986; Moorthi and Suarez 1992; Sud and Walker 1993) as well as by others in the cloud-resolving community (e.g., Xu and Randall 1996). The GATE data used for evaluating McRAS cover a 20-day period, from 30 August through 18 September 1974.

The entire model physics together with McRAS was integrated in a fully prognostic mode with the GATE data. In this mode, we also evaluated the importance of some of the subparameterizations of McRAS. Dividing the clouds into groups of shallow, middle, and upper levels is somewhat arbitrary, but when we perturbed the boundaries of such a distribution by one layer, it made very little difference to the cloud-radiative forcing. Consequently, an equal number of layers in each group was used. However, as expected, making all clouds random produces a highly erroneous cloud-radiative forcing.

Following the above, eight additional sensitivity simulations were conducted to determine the importance of the following: (a) cloud advection, (b) cloud-top entrainment instability, (c) the Cahalan (1994) correction for cloud water inhomogeneity, (d) the no-rain evaporation simulation, (e) no downdrafts, (f) the location of cloud base, (g) the 90% relative humidity criteria for the onset of convection, and (h) evaporation of clouds in downdrafts. Although these sensitivity tests are not discussed at much length here, we have determined that most of these processes help, in some way, to better simulate the GATE column environment. Indeed, we have kept even those processes that make little or no difference because we believe that the correct physics would make a difference at the appropriate place and time. Finally, we have performed a *fully prognostic* evaluation of McRAS with the GATE data. In this test, the column atmosphere was prescribed at the initial time and was forced by lateral and surface fluxes only. The results of this simulation are discussed below. The GATE data evaluation was followed by a 50-month simulation with GEOS II GCM, starting with initial data for 1 January 1987 and ending with 28 February 1991. The results of GCM evaluations are discussed in Part II. In the paper, we determine how McRAS was successful in simulating the behavior of the climate during that period.

4. Results

a. Evaluation of McRAS with GATE data

Figures 3a–j show the temperature, relative humidity, and precipitation errors (simulated minus observed) at 3-h intervals, plus several other diagnostics that cannot be verified against the observations. The McRAS simulation is remarkably accurate; it is the best ever produced by any of our cloud schemes such as shown in Sud and Walker (1993). It yields realistic time mean atmospheric soundings: temperature (Fig. 3a) and humidity (Fig. 3b), as compared to analysis of observations. In the 20-day averages, the systematic errors are very small and have virtually no systematic vertical bias. We note that there is one episode of about 4°C cooling and there is a preponderance of 1°–2°C warm (cool) patches at around the 100- (400-) hPa level, respectively. As compared to the systematic heating and cooling in Sud and Walker (1993), this is a much better simulation. In the moisture field as well, there were no systematic biases; one could infer that the model atmosphere is a little bit on the dry side, but recognizing that there is virtually no systematic temperature error and that the precipitation is less than the observed, the drier environment indicates that either the prescribed evaporation is too low or the horizontal moisture flux divergence is too high, both of which suggest that it is not a model deficiency. The fact that these errors do not relate to any systematic errors in the accompanying fields indicates that the model is performing well within the limits of observational errors.

The water and ice contributions of clouds is shown in Fig. 3c. It is diagnosed from ambient temperature following Del Genio et al. (1996). The simulated cloud fraction (Fig. 3d) and cloud optical thickness (Fig. 3e) are also realistic but remain unverifiable. Without cloud advection, these fields had a terrible structure with the isolines of constant cloudiness persisting over several days (discussed later).

The precipitation time series, shown in Fig. 3f, compares remarkably well with observations. The precipitation data for verification are derived from Q_1–Q_2 analysis of Yanai et al. (1973), although those are not too different from the radar data of Hudlow and Patterson (1979). In fact, we had produced even better simulations

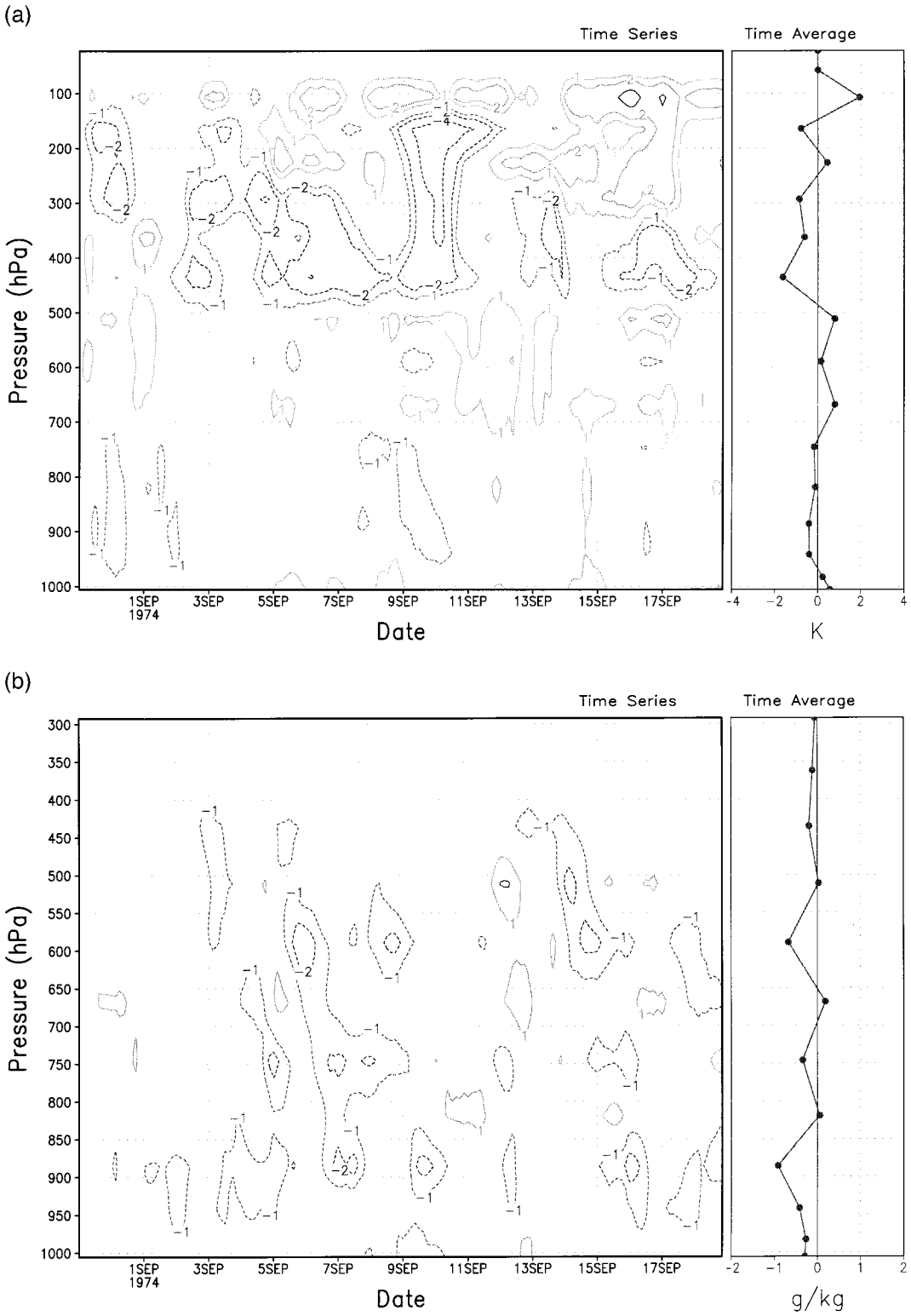

FIG. 3. Simulation with McRAS using the GATE Phase III data in a fully prognostic environment: (a) temperature (K) error; (b) specific humidity (g kg^{-1}) error;

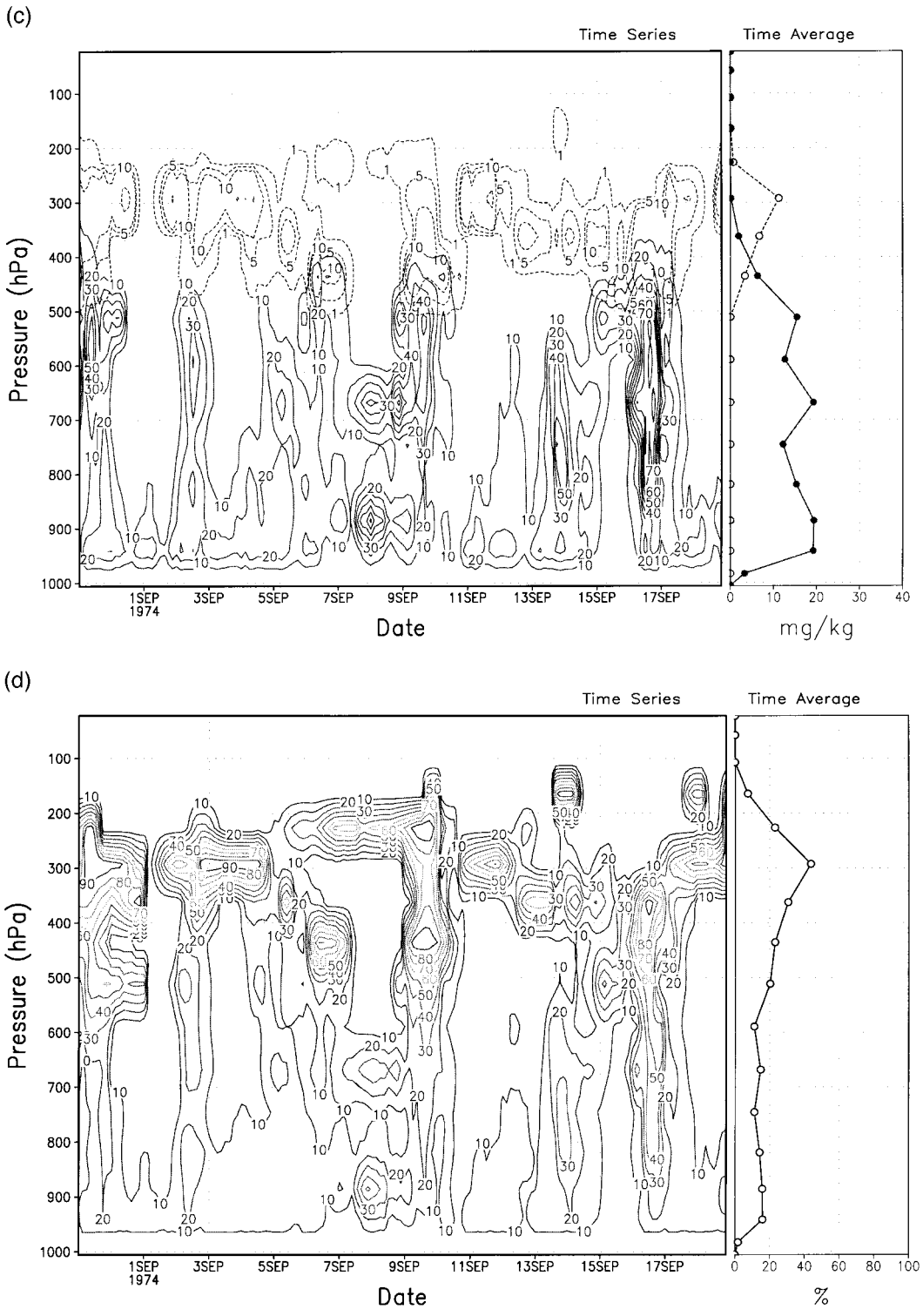

FIG. 3. (*Continued*) (c) cloud-ice and cloud water amounts (mg kg^{-1}); (d) cloud fraction (%);

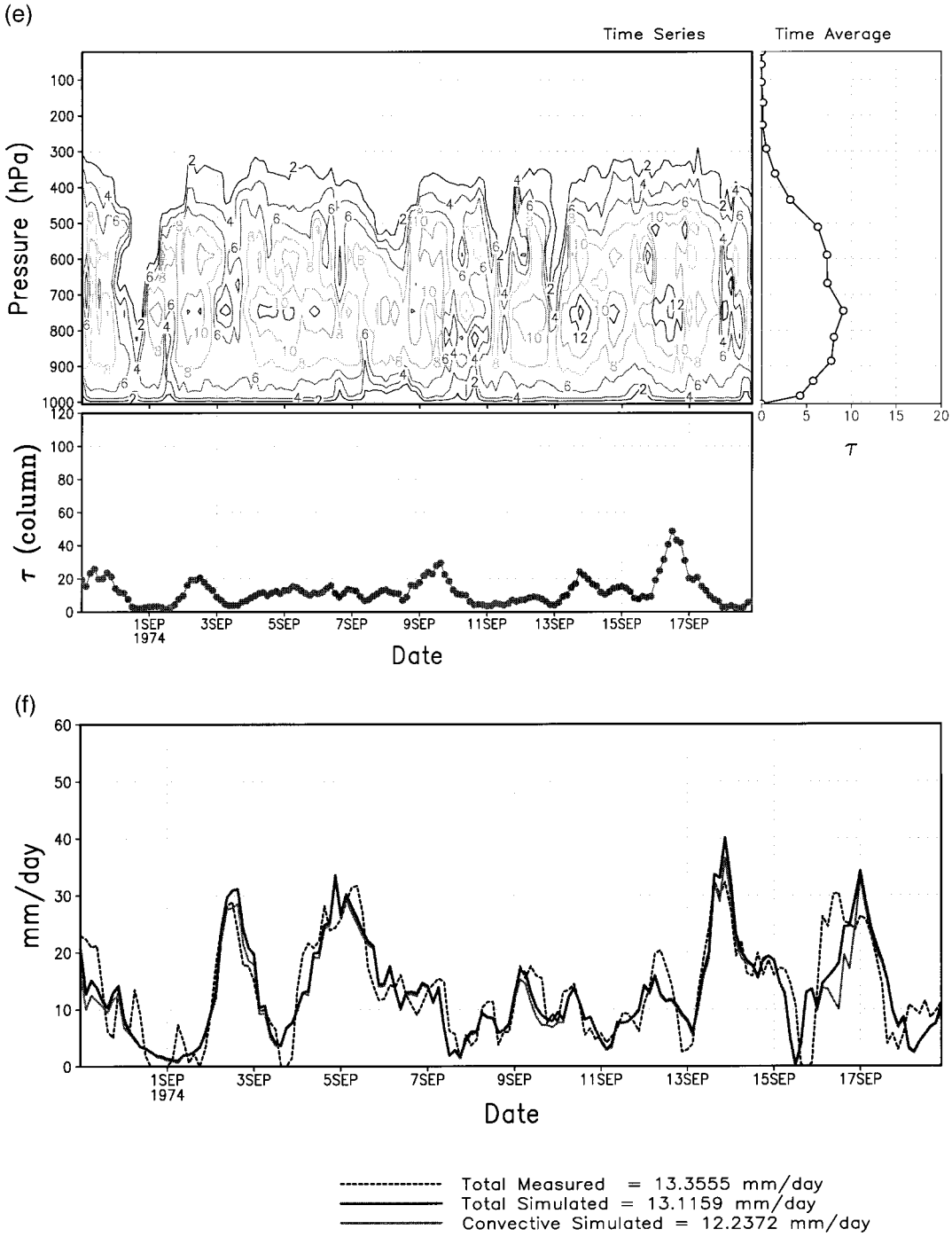

FIG. 3. (*Continued*) (e) optical thickness; (f) convective and total precipitation (mm day^{-1}) vs observations;

of precipitation [by conducting parametric sensitivity exercises with the disposable constants such as threshold relative humidity for large-scale condensation and time constant and critical cloud water constants in the precipitation production equation (29)], but here we show results produced wth McRAS using the physically defensible choice of numerical algorithms, cloud microphysical processes, and the choice of numerical constants.

Tower and anvil precipitation distribution (Fig. 3) is again realistic but unverifiable. Three preferred detrainment levels yield a jagged-looking time mean pattern of anvil precipitation, but a low precipitation yield just above and below the 500-hPa level can be expected.

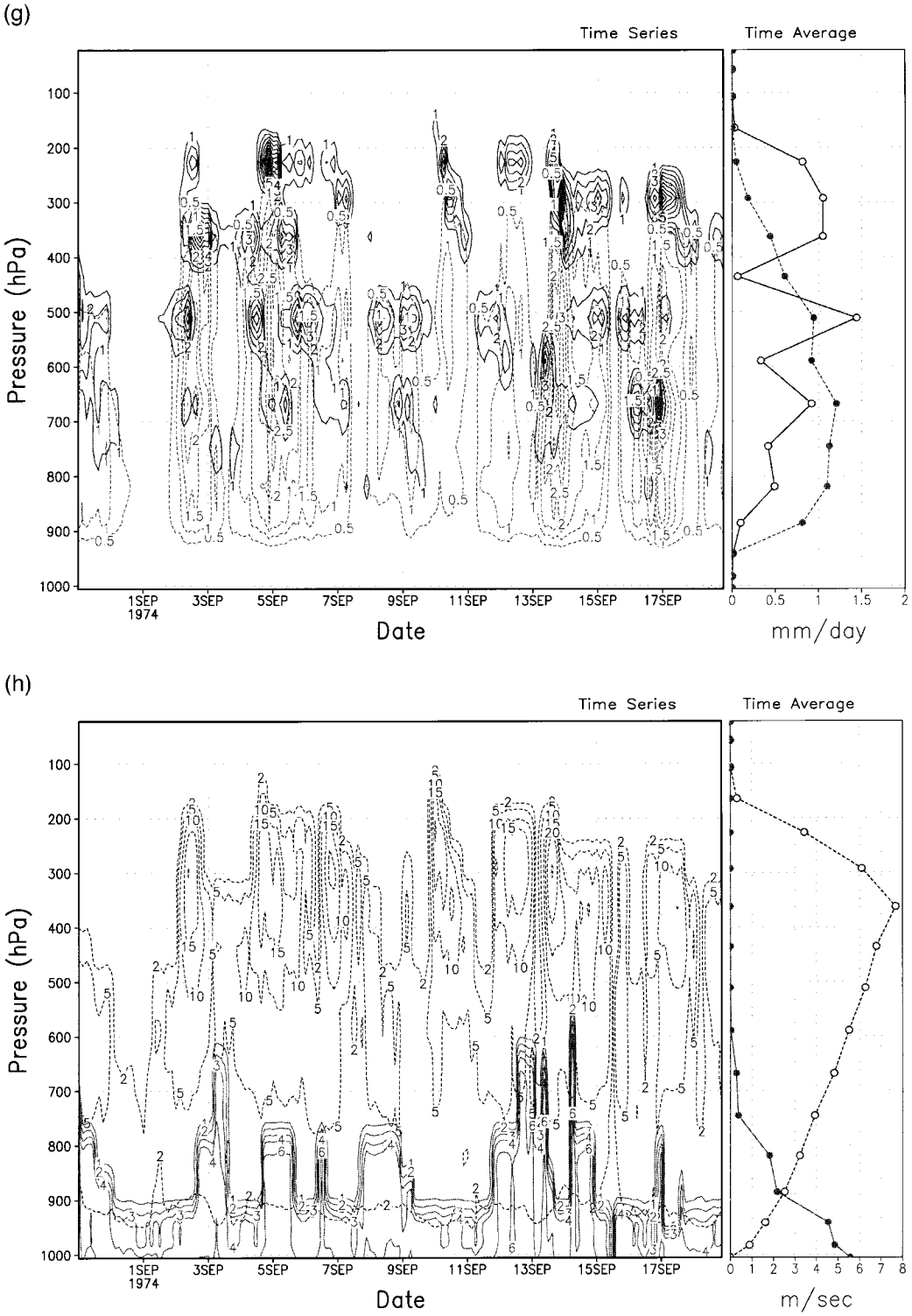

FIG. 3. (*Continued*) (g) anvil and tower precipitation (mm day^{-1}); (h) updraft and downdraft velocities (m s^{-1});

Thus, it is hard to tell whether this result is a model deficiency or a real feature of convective precipitation. We know convective clouds do produce evidence of shallow, midlevel, and deep condensation–precipitation and the output may be reflecting its structure. Future atmospheric radiation measurement (ARM) Cloud and Radiative Testbed (CART) evaluations are vital for resolving such issues.

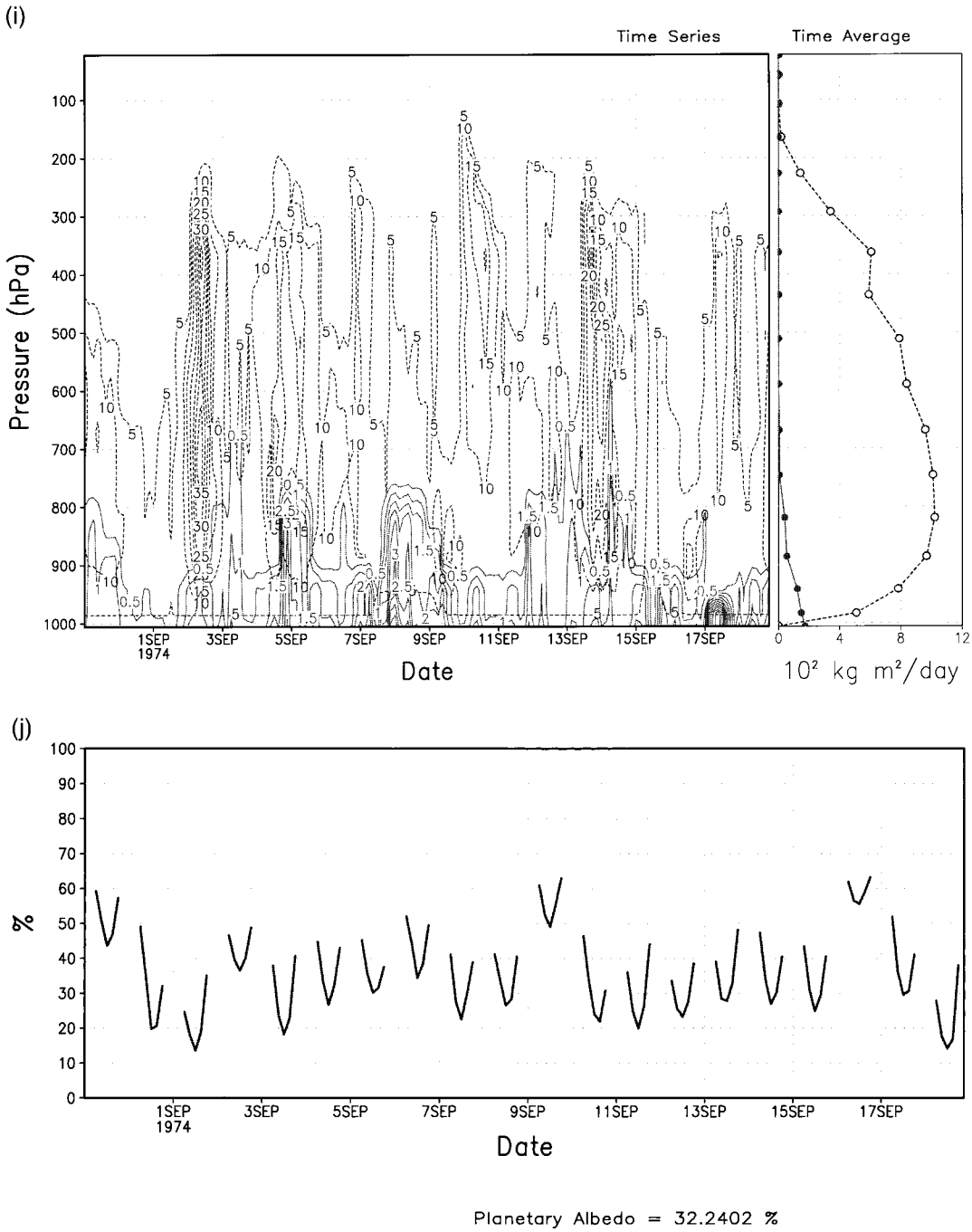

FIG. 3. (*Continued*) (i) updraft and downdraft mass fluxes (10^2 kg m^{-2} s^{-1}); and (j) planetary albedo (%). Error equals simulated minus GATE Phase III data.

McRAS also produces cumulus updraft and downdraft velocities (Fig. 3h) and mass fluxes (Fig. 3i). The time mean values are again reasonable. The downdraft mass flux seems low because nonprecipitating shallow clouds are also included in the time averages. A plot of the ratio of downdraft to the updraft mass flux gave values up to 0.65. For deep convective events, the values range from 0.25 to 0.5, which is reasonable (Sud and Walker 1993; Qian et al. 1998). The downdrafts do not produce a dramatic effect in the time averages of the oceanic environment particularly because the column atmosphere is predominantly moist adiabatic. However, in a previous GCM simulation the surface temperature differences over the United States for the boreal summer with downdrafts were 2°–4°C cooler (Sud et al. 1996). McRAS also produces realistic cloud water distribution

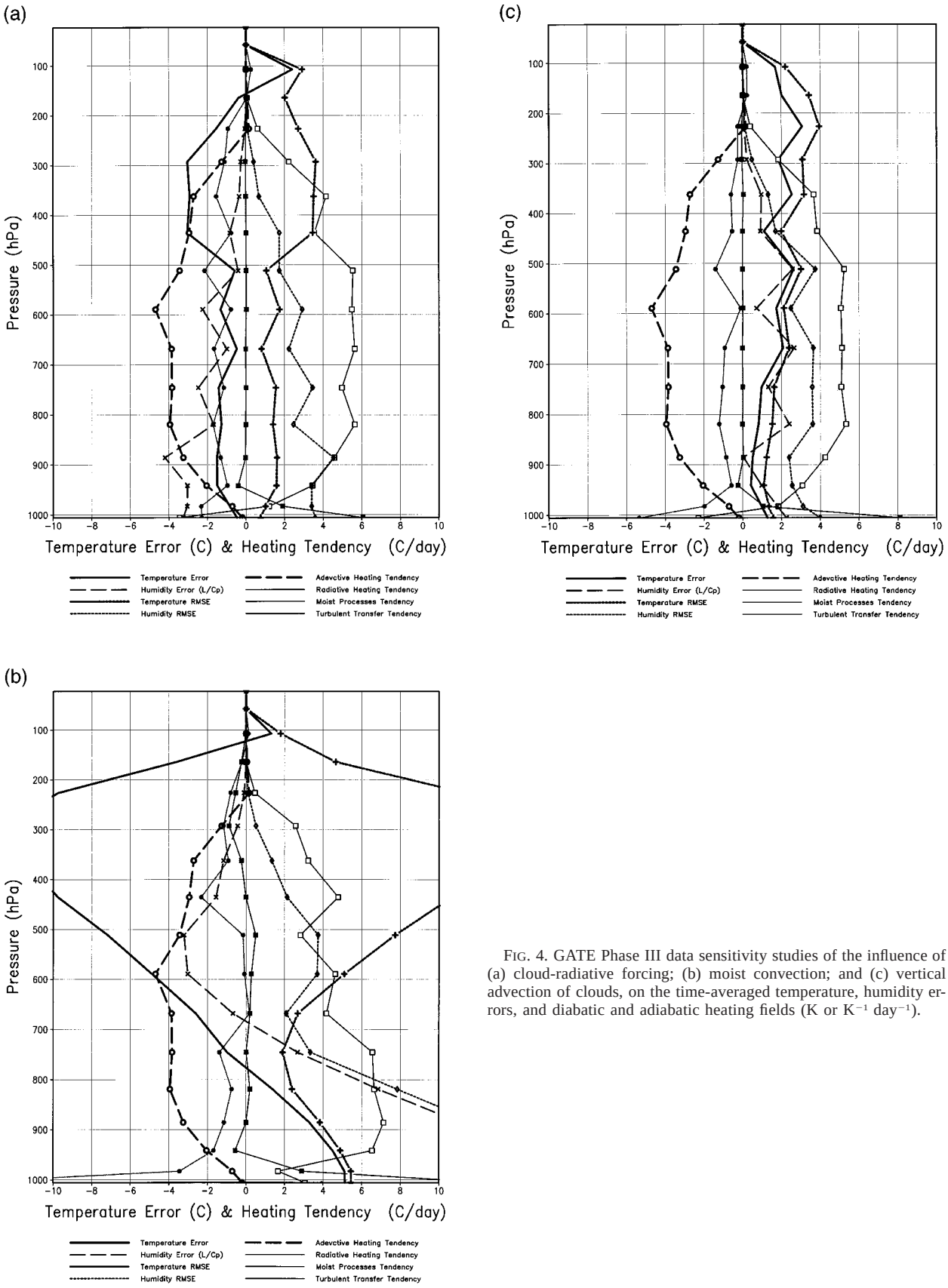

FIG. 4. GATE Phase III data sensitivity studies of the influence of (a) cloud-radiative forcing; (b) moist convection; and (c) vertical advection of clouds, on the time-averaged temperature, humidity errors, and diabatic and adiabatic heating fields (K or K^{-1} day^{-1}).

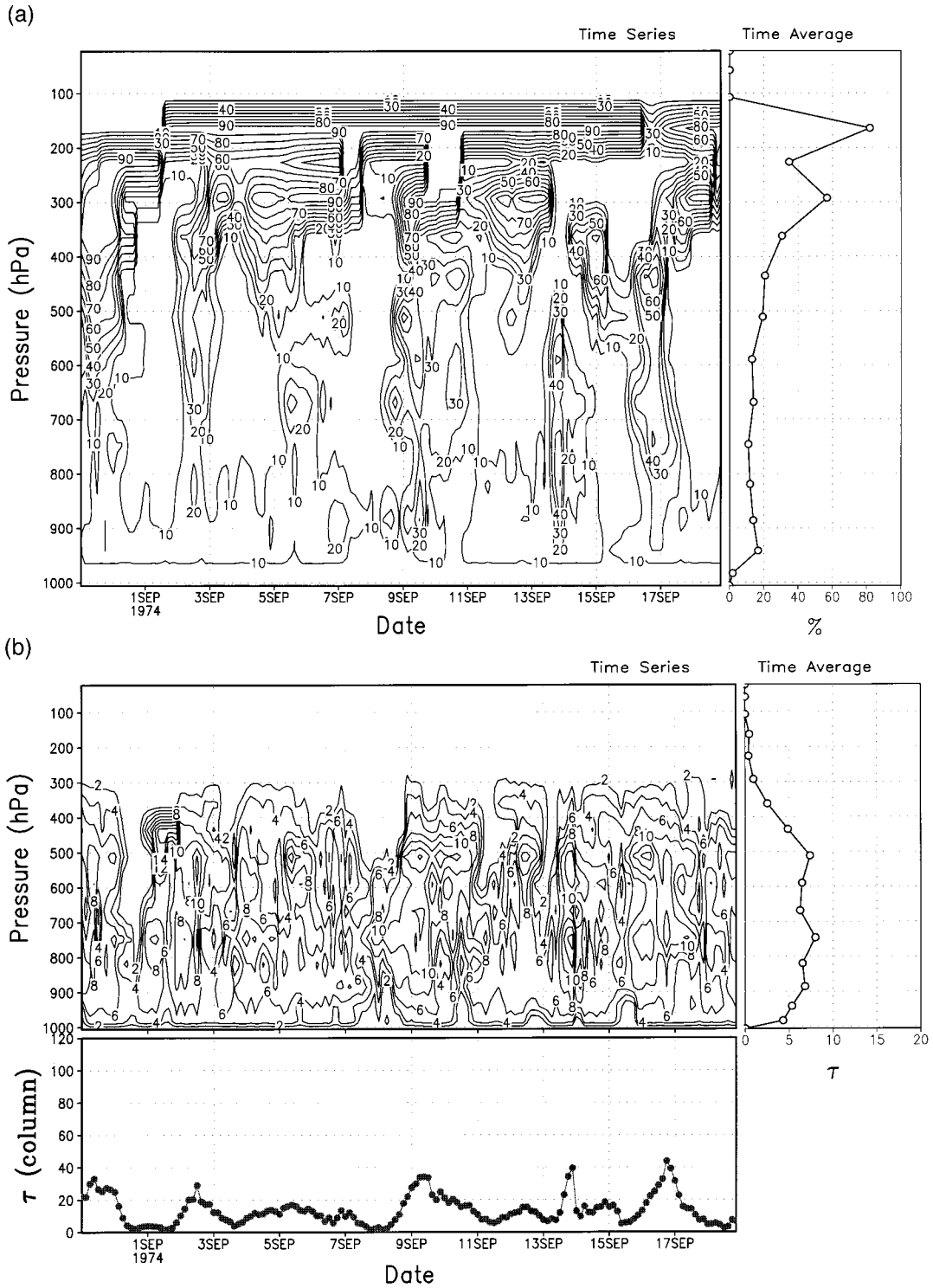

FIG. 5. Some selected subsets of plots of Fig. 3 for the GATE Phase III SCM simulation with no vertical advection of clouds. The time series of simulated (a) cloudiness, (b) cloud optical thickness,

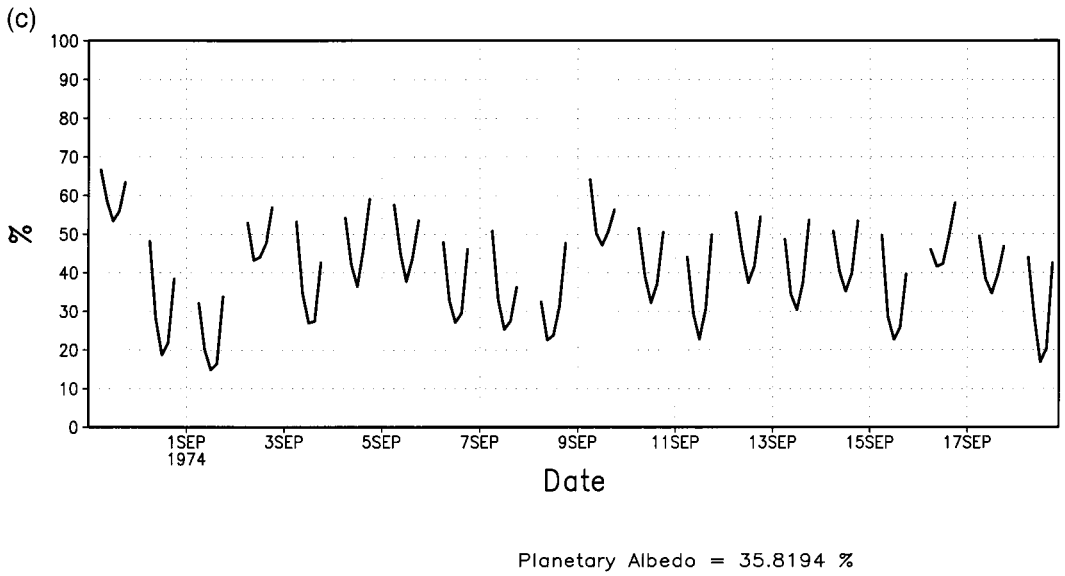

FIG. 5. (*Continued*) and (c) planetary albedo corresponds to similar plots in Fig. 3. The figure shows that no vertical advection of clouds produces persistent high clouds.

and planetary albedo (Fig. 3j); its diurnal cycle reveals the influence of solar zenith angle, while the cloud water path is implicit in the optical thicknesses.

b. Effects of cloud-radiative forcing and moist convection

In additional sensitivity tests, we found that if cloud–radiation interaction is suppressed (Fig. 4a) or moist convection (i.e., RAS) is disallowed (Fig. 4b), the model produces totally unrealistic time-mean temperature and humidity profiles. This indicates that the model physics is intimately associated with the accuracy of the time mean simulations even when the lateral forcing is unaffected; consequently the GATE data evaluation is a reliable test of model physics and its interaction with cloud schemes. This was also inferred in the previous tests by Sud and Walker (1993) and is in accord with one of the cardinal uses of SCMs as explained by Randall et al. (1996).

Disallowing cloud–radiation interaction, the average temperature of the SCM atmosphere reduces by 1°–4°C through strong radiative cooling (Fig. 4a). Such an inference is to be expected, but its magnitude is quite high despite the fact that the SST and surface fluxes remain prescribed as before and the lapse rate is nearly moist adiabatic in a strongly convective regime such as GATE Phase III. If SST feedbacks were allowed, we may get an even stronger response suggesting that cloud–radiation interaction is crucial for simulating a realistic vertical temperature profile in a SCM as well as GCM. Indeed, we know several GCMs produce a low temperature bias of 1°–2°C in the Tropics. It naturally raises the question, could errors in the cloud–radiation interaction be contributing to the bias?

Removal of RAS (Fig. 4b) introduced huge temperature errors. The lower atmosphere became warmer while the upper atmosphere became cooler. This happened because lack of convection produced most of the condensation in the boundary layer while absence of latent heating at the high levels produced the simulated cooling. Could the cooler temperatures at 500–700-hPa levels in climate simulations be related to insufficient convection? This is obviously true, but it has to be kept in mind while addressing the systematically cooler simulated troposphere in the GEOS II GCM (Sud and Walker 1999; Part II).

c. Role of vertical advection of clouds

Vertical advection of clouds is a new feature of our scheme. In the diagnostic schemes, it happens implicitly because the water vapor is advected. However, in prognostic schemes, if the clouds are not advected, they will stay in the grid cell and must dissipate locally. Indeed, clouds at high levels get advected downward with the large-scale sinking motion. Such a cloud advection has been found to eliminate persistent clouds at high levels. If the clouds are not advected in the vertical (since no horizontal advection of clouds is possible in SCM evaluation), they lead to warming in the GATE–SCM simulations (Fig. 4c). Thus, persistent high clouds compensate for the cooling that might originate from insufficient cloud–radiation interaction or moist convection. Moreover, Figs. 5a–c further demonstrate that lack of cloud advection leads to larger cloudiness at high levels because clouds, once formed there, continue to persist at those levels. The optical thickness of high clouds is small, nevertheless they contribute a few percent to the planetary albedo. In the ARM–CART tests

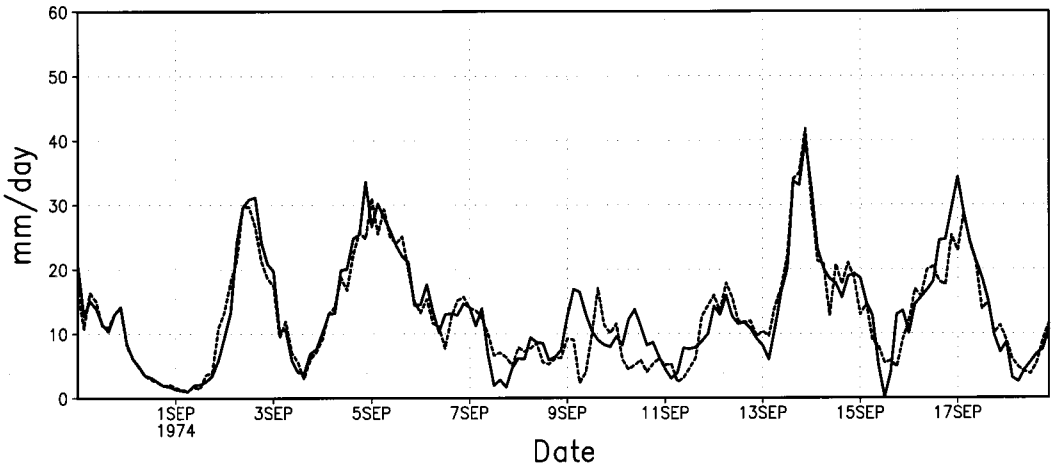

FIG. 6. Differences in precipitation produced with the original McRAS for the 17-layer model and new changes in F2 (Fig. 2a) and optical properties of ice clouds (Fig. 2b) plus adjustments to the timescale of convective clouds in GEOS II GCM.

(not shown), we found persistent clouds all through the winter in those tests in which clouds were not allowed to advect. On the other hand, inclusion of cloud advection led to better simulation of clear and cloudy days as compared to observations. However, currently the ARM–CART data are being reprocessed for more stringent internal consistency and better reliability for SCM evaluation. The reprocessed data has not been used yet. Nevertheless, ARM–CART evaluation will be carried out in the model improvement–calibration mode and reported as a separate study. At present it suffices to say that the preliminary ARM–CART evaluations reaffirmed the importance of cloud advection.

d. Treatment of cloud ice

In the current SCM evaluations, we followed Del Genio et al. (1996) for cloud–radiation interaction for both water and ice clouds. The microphysical constants and optical properties of these clouds are given in Tables 1 and 2. However, after running the new microphysics in the GCM and evaluating various systematic errors in the cloud-radiative forcing, we came across two interesting observational works: one is by Ou and Liou (1995) and the other is by Moss et al. (1996, manuscript submitted to *Quart. J. Roy. Meteor. Soc.*) as adapted by Lohmann et al. (1998). The solutions to the curve-fitted equations showed temperature-dependent relations for the physical and effective radii of ice particulates. This level of approximation is consistent with l_c or C_0 as a function of temperature. For a typical cloud-ice fraction of 5 mg kg^{-1}, the distribution of cloud particle number density has an interesting shape (shown in Fig. 2b) and is similar to the one used by Del Genio et al. (1996). Currently, this parameterization is used in the GEOS II GCM. As expected, this change produced very similar rainfall in SCM evaluations (Fig. 6) but with slightly warmer atmosphere, which in turn can be expected to reduce errors in the midlevel temperatures in the Tropics in the GCM simulations.

5. Summary and conclusions

McRAS is a new parameterization of microphysics of clouds with Relaxed Arakawa–Schubert scheme (RAS) of moist convection. RAS is the moist-convection scheme of the GEOS II GCM. We include a new parameterization for stratiform and boundary layer clouds. The microphysics of McRAS follows Sundqvist (1988), Tiedtke (1993), and Del Genio et al. (1996). Some conceptual designs are based on the work of Sundqvist (1988), Tiedtke (1993), and Del Genio et al. (1996), while various features of cloud–radiation interaction are based on the works of Chou et al. (1998, 1999) and Chou and Suarez (1994). The optical properties of cloud water and ice are from Del Genio et al. (1996). The cloud advection and diffusion are new, while cloud-top entrainment instability (CTEI) is taken from Del Genio et al. (1996). In addition, cloud microphysics in the convective towers and anvils is based on our own design while the microphysical processes still follow Sundqvist (1988).

This version of McRAS was evaluated with the GATE Phase III data in an SCM; it was implemented and evaluated in the 20-level version of the GEOS II GCM (Part II). After initial evaluations and some adjustments, the scheme performed remarkably well in GATE data evaluations. Specifically, the evaluation of predicted temperature, humidity, and precipitation fields turned out to be quite realistic even in a fully prognostic test; there are virtually no systematic errors in the time-averaged vertical profiles of humidity and temperature. If our scheme can achieve the same level of accuracy in a GCM, the assimilation of moisture would cease to be a

problem. But as long as we continue to have systematic errors in the simulated temperature and/or the moisture profiles, the data assimilation process will continue to be bogged down by problems that can, at best, be poorly resolved by nudging and/or other data-trickling techniques (Sud and Walker 1992). To eliminate such systematic errors is our top priority in improving McRAS; it will be continued with ARM–CART SCM evaluations. McRAS also produced several cloud microphysics related diagnostics. They all appear reasonable but remain unverifiable.

Three sensitivity tests were conducted to determine the importance of cloud-radiative forcing, moist convection, and cloud advection. They produced very interesting results. A cooler atmosphere will be produced by insufficient convection and/or clouds that generate lower cloud-radiative forcing particularly in the longwave, while neglect of cloud advection in the vertical tends to produce persistent high-level clouds that warm the column atmosphere. These results give some insight into solving the problem of colder middle-level tropical atmosphere, a problem that emerges in several models. McRAS is evaluated in the GEOS II GCM in Part II of our paper.

Acknowledgments. We thank K. Bergman of NASA-HQ for supporting our research. This work was undertaken on advisement from Dr. W. K.-M. Lau who has been a constant source of encouragement. We thank Dr. A. Del Genio of GISS for several useful interactions on the subject and Dr. M.-D. Chou for help with the implementation of his radiation package. Thanks are also due to Dr. S. Moorthi of NCEP for helping with understanding the nitty-gritty details in RAS.

REFERENCES

Arakawa, A., 1972: Design of the UCLA general circulation model. Tech. Rep. 7. Department of Meteorology, University of California, Los Angeles, 116 pp. [Available from Department of Meteorology, University of California, Los Angeles, Los Angeles, CA 90095.]

——, and W. H. Schubert, 1974: Interaction of cumulus cloud ensemble with the large-scale environment, Part I. *J. Atmos. Sci.,* **31,** 674–701.

Bergeron, T., 1935: On the physics of clouds and precipitation. *Proc. Fifth Assembly.* Lisbon, Portugal, UGGI, 20.

Betts, A. K., and M. J. Miller, 1986: A new convective adjustment scheme. Part II: Single column tests using GATE wave, BOMEX, ATEX and Arctic airmass data. *Quart. J. Roy. Meteor. Soc.,* **112,** 693–709.

Cahalan, R., 1994: Bounded cascade clouds: Albedo and effective thickness. *Nonlinear Processes Geophys.,* **1,** 156–167.

Cheng, M.-D., and A. Arakawa, 1997: Inclusion of rainwater budget and convective downdrafts in the Arakawa–Schubert cumulus parameterization. *J. Atmos. Sci.,* **54,** 1359–1378.

Chou, M.-D., and M. J. Suarez, 1994: An efficient thermal infrared radiation parameterization for use in general circulation models. NASA Tech. Memo. 104606, Vol. 3, 85 pp. [NTIS N95-15745.]

——, ——, C.-H. Ho, M.-H. Yan, and K.-T. Lee, 1998: Parameterization for cloud overlapping and shortwave single scattering properties for use in general circulation and cloud ensemble models. *J. Climate,* **11,** 202–214.

Chou, M.-D., K.-T. Lee, S.-C. Tsay, and Q. Fu, 1999: Parameterization for cloud longwave scattering for use in atmospheric models. *J. Climate,* **12,** 159–169.

Deardorff, J. W., 1976: On entrainment rate of stratocumulus topped mixed layer. *Quart. J. Roy. Meteor. Soc.,* **102,** 563–582.

——, 1980: Cloud-top entrainment instability. *J. Atmos. Sci.,* **37,** 131–147.

Del Genio, A. D., N.-S. Yao, W. Kovari, and K. K.-W. Lo, 1996: A prognostic cloud water parameterization for general circulation models. *J. Climate,* **9,** 270–304.

Emanuel, K. A., J. D. Neelin, and C. S. Bretherton, 1994: On large scale circulation in convective atmospheres. *Quart. J. Roy. Meteor. Soc.,* **120,** 1111–1143.

Fowler, L. D., and D. A. Randall, 1996a: Liquid and cloud ice microphysics in the CSU GCM. Part II: Impact of cloudiness, the earth's radiation budget, and general circulation of the atmosphere. *J. Climate,* **9,** 530–560.

——, and ——, 1996b: Liquid and cloud ice microphysics in the CSU GCM. Part III: Sensitivity to modeling assumptions. *J. Climate,* **9,** 561–586.

——, ——, and S. A. Rutledge, 1996: Liquid and cloud ice microphysics in the CSU GCM. Part I: Model description and simulated microphysical processes. *J. Climate,* **9,** 489–529.

Fu, Q., 1996: An accurate parameterization of the solar radiative properties of cirrus clouds for climate models. *J. Climate,* **9,** 2058–2082.

Gadgil, S., and S. Sajani, 1991: Monsoon precipitation in AMIP runs (results from an AMIP diagnostic subgroup). *Climate Dyn.,* **14,** 659–689.

Helfand, H. M., and J. C. Lebraga, 1988: Design of a nonsingular level 2.5 second-order closure model for prediction of atmospheric turbulence. *J. Atmos. Sci.,* **45,** 113–132.

Hudlow, M. D., and V. L. Patterson, 1979: GATE radar rainfall atlas. NOAA Special Rep. USGPO 003-019-00046-2, Center for Environmental Assessment Service, NOAA, 155 pp.

Kessler, E., 1969: On the distribution and continuity of water substance in the atmospheric circulation. *Meteor. Monogr.,* No. 32, Amer. Meteor. Soc., 84 pp.

Kinzer, G. D., and R. Gunn, 1951: The evaporation temperature and thermal relaxation time of freely falling water drops. *J. Meteor.,* **8,** 71–83.

Krishnamurti, T. N., S. Low-Nan, and R. Pasch, 1983: Cumulus parameterization and rainfall rates II. *Mon. Wea. Rev.,* **11,** 815–828.

Kuo, Y.-H., and R. Anthes, 1984: Semiprognostic tests of Kuo-type cumulus parameterization schemes in an extratropical convective system. *Mon. Wea. Rev.,* **112,** 1498–1505.

LeTreut, H., and Z. X. Li, 1988: Using meteosat data to validate a prognostic cloud scheme. *Atmos. Res.,* **21,** 273–292.

Lin, S.-J., and R. B. Rood, 1996: Multidimensional flux-from semi-Lagrangian transport schemes. *Mon. Wea. Rev.,* **124,** 2046–2070.

Lohmann, U., N. McFarlane, L. Levkov, and K. Abdella, 1999: Comparing different cloud schemes of a single column model by using mesoscale forcing and nudging technique. *J. Climate,* **12,** 438–461.

Lord, S. J., 1978: Development and observational verification of a cumulus cloud parameterization. Ph.D. dissertation, University of California, Los Angeles, 359 pp.

——, 1982: Interaction of a cumulus cloud ensemble with the large-scale environment. Part III: Semi-prognostic test of the Arakawa–Schubert cumulus parameterization. *J. Atmos. Sci.,* **39,** 88–103.

——, W. C. Chao, and A. Arakawa, 1982: Interaction of a cumulus cloud ensemble with the large-scale environment. Part IV: The discrete model. *J. Atmos. Sci.,* **39,** 104–113.

Manabe, S., and J. L. Holloway Jr., 1971: Simulation of climate by a global general circulation model. Hydrologic cycle and heat balance. *Mon. Wea. Rev.,* **99,** 335–369.

Marshall, J. S., and W. M. Palmer, 1948: The distribution of raindrops with size. *J. Meteor.,* **5,** 165–166.
Mocko, D. M., and W. A. Cotton, 1995: Evaluation of fractional cloudiness parameterizations for use in a mesoscale model. *J. Atmos. Sci.,* **52,** 2884–2901.
Moorthi, S., and M. J. Suarez, 1992: Relaxed Arakawa–Schubert: A parameterization of moist convection for general circulation models. *Mon. Wea. Rev.,* **120,** 978–1002.
Moss, S. J., and D. W. Johnson, 1995: The calculation and parameterization of effective radius of ice-particles using aircraft data. *IUGG 21st General Assembly,* Boulder, CO, IUGG.
Ou, S. C., and K. N. Liou, 1995: Ice microphysics and climate temperature feedback. *Atmos. Res.,* **35,** 127–138.
Qian, L., G. S. Young, and W. M. Frank, 1998: A convective wake parameterization scheme for use in general circulation models. *Mon. Wea. Rev.,* **126,** 456–469.
Randall, D. A., 1980: Conditional instability of first kind upside-down. *J. Atmos. Sci.,* **37,** 125–130.
——, 1989: Cloud parameterization for climate models: Status and prospects. *Atmos. Res.,* **23,** 341–361.
——, K.-M. Xu, R. C. J. Somerville, and S. Iscobellis, 1996: Single-column models and cloud ensemble models as links between observations and climate models. *J. Climate,* **9,** 1683–1697.
——, and W. B. Wielicki, 1997: Measurements, models, and hypotheses in atmospheric science. *Bull. Amer. Meteor. Soc.,* **78,** 399–405.
Rasch, P. J., and J. E. Kristjansson, 1997: A comparison of CCM3 model climate using diagnosed and predicted condensate parameterizations. *J. Climate,* **11,** 1587–1614.
Rogers, R. R., and M. K. Yau, 1989: *A Short Course in Cloud Physics.* Pergamon, 293 pp.
Schlesinger, M. E., and J.-H. Oh, 1993: A cloud-evaporation parameterization for general circulation models. *Mon. Wea. Rev.,* **121,** 1239–1248.
Simpson, J. 1971: On cumulus entrainment and one-dimensional models. *J. Atmos. Sci.,* **28,** 449–455.
——, and V. Wiggert, 1971: 1968 Florida cumulus seeding experiment: Numerical model results. *Mon. Wea. Rev.,* **99,** 87–118.
Slingo, J., 1987: The development and verification of a cloud prediction scheme for the ECMWF model. *Quart. J. Roy. Meteor. Soc.,* **113,** 899–927.
Suarez, M. J., and L. L. Takacs, 1995: Documentation of Aires/GEOS dynamical core version 2. NASA Tech. Memo. 104606, Vol. 5, 44 pp. [Available from Goddard Space Flight Center, Greenbelt, MD 20771.]
Sud, Y. C., and G. K. Walker, 1992: A review of recent research on improvement of physical parameterizations in the GLA GCM. *Physical Processes in Atmospheric Models,* D. R. Sikka and S. S. Singh, Eds., Wiley, 422–479.
——, and ——, 1993: A rain evaporation and downdraft parameterization to complement a cumulus updraft scheme and its evaluation using GATE data. *Mon. Wea. Rev.,* **121,** 3019–3039.
——, and ——, 1999: Microphysics of clouds with the Relaxed Arakawa–Schubert Scheme (McRAS). Part II: Implementation and Performance in GEOS II GCM. *J. Atmos. Sci.,* **56,** 3221–3240.
——, W. C. Chao, and G. K. Walker, 1991: Contribution to the implementation of Arakawa–Schubert cumulus parameterization in the GLA GCM. *J. Atmos. Sci.,* **48,** 1573–1586.
——, K.-M. Lau, R. Yang, J. Zhou, G. K. Walker, and J.-H. Kim, 1996: Climatology of circulation and hydrologic processes in the AMIP simulation with the GLA GCM. *Proc. First Int. AMIP Scientific Conference,* Geneva, Switzerland, World Meteorological Organization, 65–69.
Sundqvist, H., 1978: A parameterization of non-convective condensation including prediction of cloud water content. *Quart. J. Roy. Meteor. Soc.,* **104,** 677–690.
——, 1988: Parameterization of condensation and associated clouds in models for weather prediction and general circulation simulation. *Physically Based Modelling and Simulation of Climate and Climatic Change,* M. E. Schlesinger, Ed., Reidel, 433–461.
——, 1993: Inclusion of ice-phase of hydrometeors in cloud parameterization of large-scale and meso-scale models. *Contrib. Atmos. Phys.,* **66,** 137–147.
——, E. Berge, and J. E. Kristjansson, 1989: Condensation and cloud parameterization studies with a mesoscale numerical weather prediction model. *Mon. Wea. Rev.,* **117,** 1641–1657.
Takacs, L. L., A. Molod, and T. Weng, 1994: Goddard Earth Observing System (GEOS) general circulation model (GCM) version 1. NASA Tech. Memo. 104606, Vol. 1, 97 pp. [Available from NASA/Goddard Space Flight Center, Greenbelt, MD 20771.]
Tiedtke, M., 1993: Representation of clouds in large-scale models. *Mon. Wea Rev.,* **121,** 3040–3061.
Tsay, S.-C., K. Stamens, and K. Jayaweera, 1989: Radiative energy balance in the cloudy and hazy Arctic. *J. Atmos. Sci.,* **46,** 1002–1018.
Wang, W., and M. E. Schlesinger, 1995: The dependence on convective parameterization of tropical intraseasonal oscillations—An assessment using the UIUC GCM. *Proc. First Int. AMIP Scientific Conf.,* Geneva, Switzerland, World Meteorological Organization, 125–130.
——, and ——, 1999: The dependence on convection parameterization of the tropical intraseasonal oscillation simulated by the 11-layer UIUC atmospheric GCM. *J. Climate,* **12,** 1423–1457.
Washington, W. M., and A. Kasahara, 1970: A January simulation experiment with the two-layer version of the NCAR global circulation model. *Mon. Wea. Rev.,* **98,** 559–580.
Witting, P. J., 1995: Numerical investigation of stratus cloud layer breakup by cloud top instabilities. Ph.D. dissertation, Stanford University, 201 pp.
Xu, K.-M., and D. A. Randall, 1996: A semiempirical cloudiness parameterization for use in climate models. *J. Atmos. Sci.,* **53,** 3084–3102.
Yanai, M., S. Esbensen, and J.-H. Chu, 1973: Determination of bulk properties of tropical cloud clusters from large-scale heat and moisture budgets. *J. Atmos. Sci.,* **30,** 611–627.
Zhang, M. H., and J. L. Lin, 1997: Constrained variational analysis of sounding data based on column-integrated budgets of mass, heat, moisture, and momentum: Approach and application to ARM measurements. *J. Atmos. Sci.,* **54,** 1503–1524.
Zhao, Q., and F. H. Carr, 1997: A prognostic cloud scheme for NWP models. *Mon. Wea Rev.,* **125,** 1931–1953.